Behavioral Modeling of Viscous Damping in MEMS

Satish Vemuri

2000

Advisor: Prof. Fedder/Mukheriee

Electrical & Computer ENGINEERING

Report Documentation Page

1. REPORT DATE **2000**	2. REPORT TYPE	3. DATES COVERED **00-00-2000 to 00-00-2000**

4. TITLE AND SUBTITLE **Behavioral Modeling in Viscous Damping in MEMS**	5a. CONTRACT NUMBER
	5b. GRANT NUMBER
	5c. PROGRAM ELEMENT NUMBER
6. AUTHOR(S)	5d. PROJECT NUMBER
	5e. TASK NUMBER
	5f. WORK UNIT NUMBER

7. PERFORMING ORGANIZATION NAME(S) AND ADDRESS(ES) **Carnegie Mellon University,Department of Electrical and Computer Engineering,Pittsburgh,PA,15213-3890**	8. PERFORMING ORGANIZATION REPORT NUMBER

9. SPONSORING/MONITORING AGENCY NAME(S) AND ADDRESS(ES)	10. SPONSOR/MONITOR'S ACRONYM(S)
	11. SPONSOR/MONITOR'S REPORT NUMBER(S)

12. DISTRIBUTION/AVAILABILITY STATEMENT **Approved for public release; distribution unlimited**

13. SUPPLEMENTARY NOTES

14. ABSTRACT **see report**

15. SUBJECT TERMS

16. SECURITY CLASSIFICATION OF:			17. LIMITATION OF ABSTRACT	18. NUMBER OF PAGES	19a. NAME OF RESPONSIBLE PERSON
a. REPORT **unclassified**	b. ABSTRACT **unclassified**	c. THIS PAGE **unclassified**	**Same as Report (SAR)**	**45**	

Behavioral Modeling of Viscous Damping in MEMS

M.S. Thesis Report

by

Satish Kumar Vemuri

Department of Electrical and Computer Engineering

Carnegie Mellon Univeristy

Committee

Prof. Gary K. Fedder

Dr. Tamal Mukherjee

Acknowledgements

Table of contents

1. Introduction

MicroElectroMechanicalSystems (MEMS) are often characterized by structures that are a few microns in size, separated by micron-sized gaps. At these sizes and gaps, viscous air damping dominates other energy dissipation mechanisms at atmospheric pressure, thus, affecting the dynamic behavior of the devices. Also, the number of such gaps can be very large in a MEMS device. Hence, fast and accurate behavioral simulation of the dynamics of MEMS systems necessitates accurate, low-order damping models. Further, to be useful in the design flow, these models need to be parameterized, so that they can be used to model damping for a wide range of structure size, gap, frequency and amplitude of motion.

Viscous damping due to the fluid surrounding the moving structures can be of two types: squeeze film damping and lateral damping. In squeeze film damping, there are two parallel structures as shown in Fig. 1.1. They are in relative motion perpendicular to the plane, thus squeezing the air film between the structures. The air counters the motion by exerting an opposing force. Fig. 1.2 shows the case of lateral damping. Here the motion of the plate is parallel to the plane of the structure. The resulting fluid flow causes energy dissipation and exerts an opposing force which is a function of the velocity of the moving plate, the dimensions of the plate, its distance from other parallel structures, and the viscosity of the fluid.
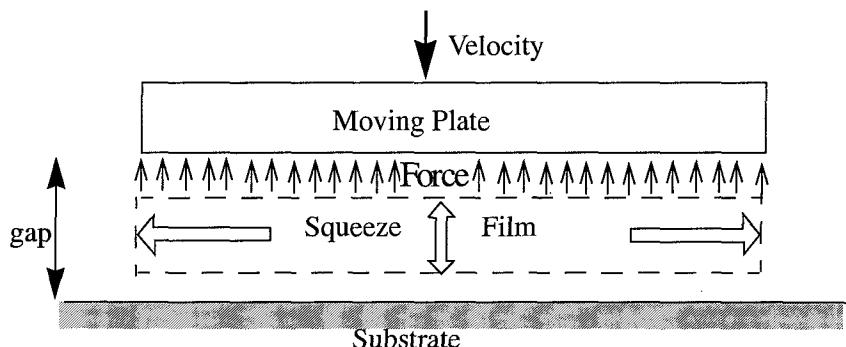
Fig. 1.1: Cross section of a squeeze film between a moving plate and the substrate

This report presents lumped parameter models for squeeze film and lateral damping. The accuracy of these models down to MEMS scaled structures, and their parameterized nature makes them useful for design and simulation of MEMS devices. With the edge-effect contribution to the
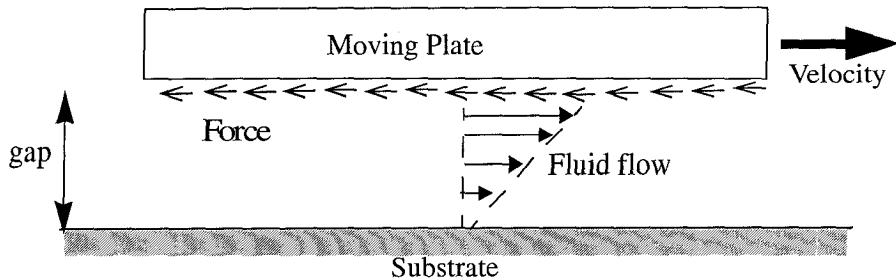
Fig. 1.2: Cross section of a moving plate that is laterally damped

damping force becoming significant in micron-scaled structures, emphasis is laid on including these effects.

In chapter 2, squeeze film damping model is discussed. Finite element simulations of squeeze film are presented. The derivation of the behavioral model for squeeze film from existing analytical model [1] and its extension to include the edge and the finite-size effects are discussed. The significance of the contribution of these effects for MEMS scaled devices is established. The edge-effects enhanced behavioral model is evaluated, for varying frequency, amplitude of plate motion and the aspect ratio of the plate by comparing it with FEM simulations. Simulation results for a square wave input are presented.

In chapter 3, modeling of the fluid flow invoked by a laterally moving structure and the derivation of the behavioral model for lateral damping are discussed. The accuracy of the behavioral model is quantified by comparison with the finite element simulations. Simulation results for a square wave input and for varying aspect ratio and oscillation frequency are discussed.

Chapter 4 establishes the use of the presented damping models in system level simulation and design, by use in the nodal simulation of a bandpass filter and a lateral resonator. The simulation results are compared with the experimental results which establishes the accuracy of the damping models.

Finally, chapter 5 concludes the overall work and discusses some future work that could be done in this direction.

2. Squeeze film damping

2.1 Introduction

When a fluid film between two parallel surfaces is squeezed by the relative motion of the surfaces towards each other, a force that opposes the motion of the structures is produced. This type of energy dissipation mechanism, called squeeze film damping, is encountered very commonly in MEMS devices. A squeeze film is characterized by physical dimensions like width, length and thickness of the fluid film that is squeezed. Other parameters that determine the damping are the ambient pressure, the temperature of device operation, viscosity coefficient of the fluid and the velocity of the oscillating plate.

Example applications include MEMS systems that have a proof mass oscillating vertically above a static bottom plane or a differential comb drive. Damping of the proof mass in a z-axis accelerometer is a fundamental consideration in the design of the accelerometer. In differential comb drives, the squeezed air between the stator and the rotor fingers contributes most of the damping in the differential comb drives. Fig. 2.1 shows the squeeze film between the stator and rotor fingers of a differential comb drive. The stator finger moves in the direction marked in Fig. 2.1 (b). The thickness of the structure is equal to the width of the squeeze film (typically a few microns); the overlap distance of the stator and rotor fingers is equal to the length of the squeeze film (tens of microns); and the equilibrium gap between the stator and the rotor fingers is equal to the gap between the top and the bottom plate (typically a couple of microns).


(a) (b)
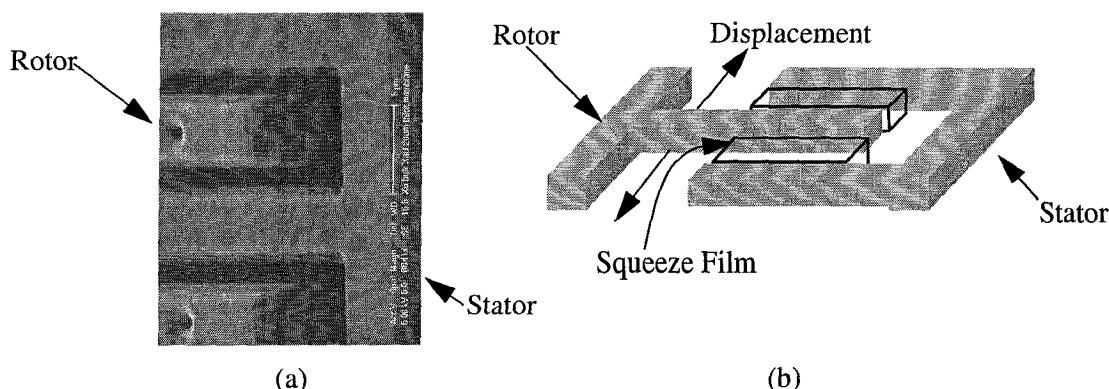
Fig. 2.1 (a): SEM picture showing the stator and the rotor fingers of a differential comb drive
(b): Picture showing the squeeze film between the stator and rotor fingers

2.2 Squeeze film model

2.2.1 Squeeze film physics

The gas pressure distribution across the moving plate, as a result of squeeze film effect, is governed by the Reynolds equation. Under isothermal conditions, the pressure (that is close to ambient pressure) is inversely proportional to the volume occupied by the gas, or, directly proportional to the density of the gas. When the plates are parallel and the relative displacement of the moving plate is small as compared to the distance between the plates, the second-order, non-linear partial differential equation simplifies to the linearized Reynolds equation (EQ. 2.1) and to EQ. 2.2 under isothermal conditions [2, 3].

$$\frac{\partial}{\partial x}\left(\rho g^3 \frac{\partial p}{\partial x}\right) + \frac{\partial}{\partial y}\left(\rho g^3 \frac{\partial p}{\partial y}\right) = 12\eta \frac{\partial(\rho g)}{\partial t} \qquad \text{EQ. 2.1}$$

$$\frac{P_a g^2}{12\eta}\left(\frac{\partial^2}{\partial x^2} + \frac{\partial^2}{\partial y^2}\right)\left(\frac{p}{P_a}\right) - \frac{\partial}{\partial t}\left(\frac{p}{P_a}\right) = \frac{\partial}{\partial t}\left(\frac{z}{g}\right) \qquad \text{EQ. 2.2}$$

where ρ is the density of the gas, p is the change in pressure from the ambient pressure, P_a is the ambient pressure, g is the gap between the plates, η is the viscosity coefficient of air and z is the vertical displacement of the moving plate, x and y are the cartesian coordinates.

2.2.2 Gas rarefaction effects

The squeeze film sizes that are found in MEMS devices may result in a condition where the fluid film can no longer be considered to be within continuum limits. As the film thickness is reduced, the mean-free path of the molecules becomes significant as compared to the critical dimension, which is the squeeze film thickness in this case. This regime of operation can be given by a dimensionless quantity called the Knudsen number, K_n, which is the ratio of the mean free path of the gas molecules under consideration λ, to the gap between the plates, g. When $K_n < 1/100$, the fluid can be considered to be in the continuum limits and the no-slip assumption that the plate velocity and the fluid velocity at plate surface is equal remains valid. On the other end, if $K_n > 1$, then molecular regime of operation should be considered. Slip conditions begin to occur when λ becomes a fraction of g (>1/100). The mean free path of air is about 70 nm at standard temperature and pressure. The gaps that are commonly encountered in squeeze film damping

can be a couple of microns. So slip conditions have to be taken into account. At lower pressures K_n is higher because λ increases, and the region of operation shifts more and more towards the molecular regime.

The effect of slip-conditions can be modeled by using a value of effective viscosity which is lower than the actual viscosity of the fluid. There are many existing equations to model the viscosity of the fluid flowing in a narrow channel as summarized in [3]. We use the value pointed to by Veijola et al. [3]. The equation for effective viscosity is given by:

$$\eta_{eff} = \frac{\eta}{1 + 9.638 K_n^{1.159}}$$

EQ. 2.3

where η_{eff} is the effective viscosity, η is the fluid viscosity, K_n is the Knudsen number. Fig. 2.2 plots the effective viscosity as a function of gap between the plates. the decrease in the effective viscosity can be seen with decreasing gap.
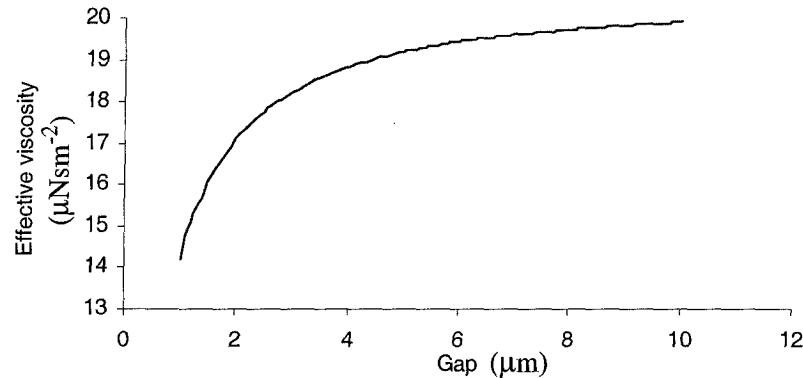
Fig. 2.2: Effective viscosity as a function of gap

2.2.3 Squeeze force: Solution to compressible, linearized Reynolds equation

The linearized Reynolds equation (EQ. 2.2) can be solved under compressible conditions for sinusoidal oscillation of the a rectangular plate. The solution consists of a spring force in phase with the plate displacement and a damping force in phase with the plate velocity[Blechs]. The inte-

gral of the gauge pressure over the area of the plate gives the following relations for the damping and the spring forces [1]:

$$\frac{F_d}{z} = \frac{64\sigma P_a wl}{\pi^4 g} \sum_{\substack{m,n \\ odd}} \frac{m^2 + n^2 c^2}{(mn)^2 \{[m^2 + n^2 c^2]^2 + \sigma^2/\pi^4\}}$$ EQ. 2.4

$$\frac{F_s}{z} = \frac{64\sigma^2 P_a wl}{\pi^8 g} \sum_{\substack{m,n \\ odd}} \frac{1}{(mn)^2 \{[m^2 + n^2 c^2]^2 + \sigma^2/\pi^4\}}$$ EQ. 2.5

where F_d and F_s are the damping and spring forces, l is the length, w is the width and c is the aspect ratio of the plate (width/length), z is the amplitude of motion, g the gap and σ is the squeeze number given by:

$$\sigma = \frac{12\eta_{eff} w^2 \omega}{P_a g^2}$$ EQ. 2.6

where ω is the angular frequency of oscillation.

2.3 Finite element simulation of squeeze film

Finite element simulations of the dynamics of squeeze films are performed using a code which solves three-dimensional Navier-Stokes equation. One such commercial code used in this thesis is CFD-ACE [4, 5]. Transient simulations of a plate oscillating vertically above an infinite substrate are performed. The damping force on the oscillating plate is determined by the integration of the gauge pressure (pressure deviation from the ambient pressure) over the surface of the oscillating plate.

To verify the finite element simulations, a well known and analyzed problem was solved. A square plate of size 1mm on a side, oscillating with an amplitude of 0.1 μm and a frequency of 1 kHz was chosen. Fig 2.3 shows the damping force with time for a gap of 2 μm. The damping coefficient can be extracted from the peak force. The analytical equation for the damping coefficient for a square plate of length l on a side and a gap g, is given by EQ. 2.7 [6].

$$B = 0.422 \frac{\eta_{eff} l^4}{g^3}$$ EQ. 2.7

where η_{eff} is the effective viscosity coefficient of the fluid.

The values of damping coefficient obtained from the FEA method with ambient pressure set at the plate edges and the analytical method are 0.96 and 1.0 respectively. They match to within 4% which verifies and quantifies the accuracy of the finite element simulations.
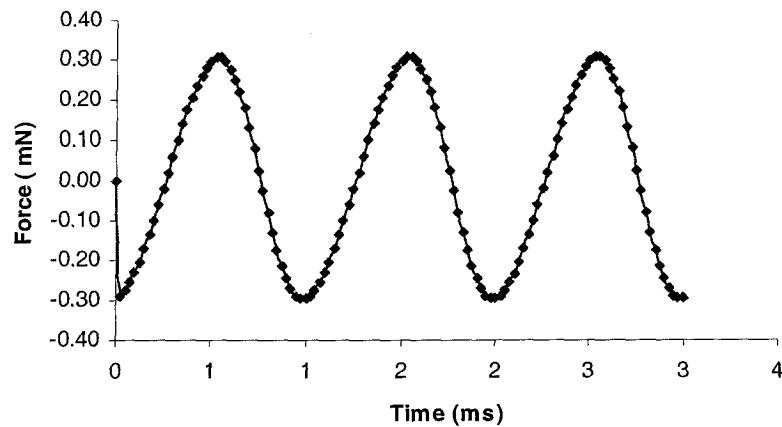
Fig. 2.3: Damping force on a sinusoidally oscillating plate

The accuracy of the finite element simulations also depends on the boundary conditions used. Two different boundary conditions can be used in the simulation of the squeeze film damping: trivial boundary conditions and non-trivial boundary conditions. The advantages of each approach is discussed next.
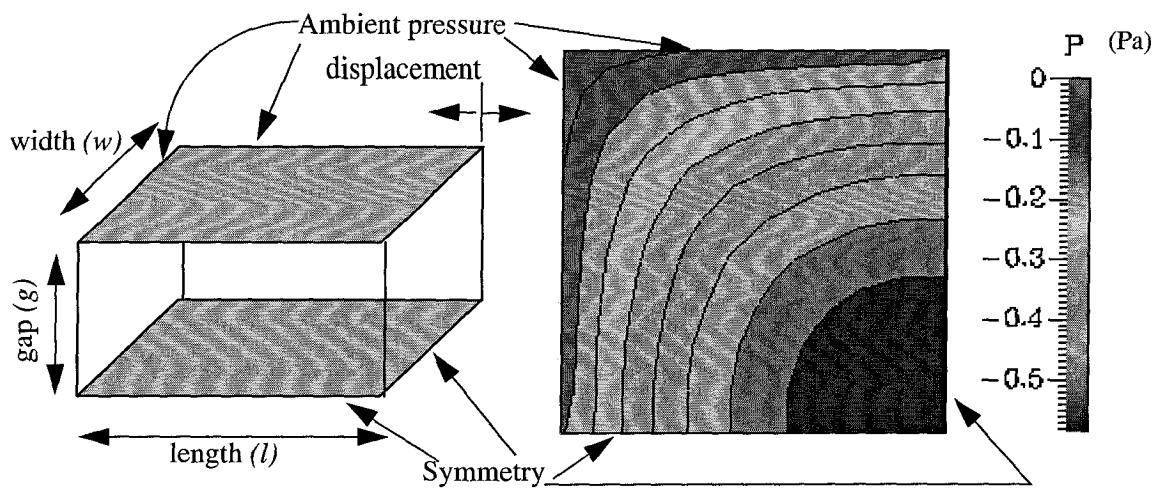
(a): Squeeze film with TBC   (b): Pressure distribution across top plate

Fig. 2.4: 20 μm square plate oscillating with 0.1 μm amplitude at 1 kHz

2.3.1 Trivial boundary conditions

In trivial boundary conditions, the squeeze film space is represented by a 3-D grid between an oscillating plate and substrate as shown in Fig. 2.4 (a). To exploit the symmetry conditions for reducing the number of grid cells and the computer resources in terms of memory and CPU time, only a quarter section of the squeeze film is used in simulations. Ambient pressure boundary condition is used at the plate edges. Fig. 2.4.b shows the pressure distribution across a the quarter plate when a square plate of size 20 μm is oscillating sinusoidally with an amplitude of 0.1 μm and a frequency of 1 kHz. It can be noticed that the gauge pressure is forced to zero at the plate-edges.
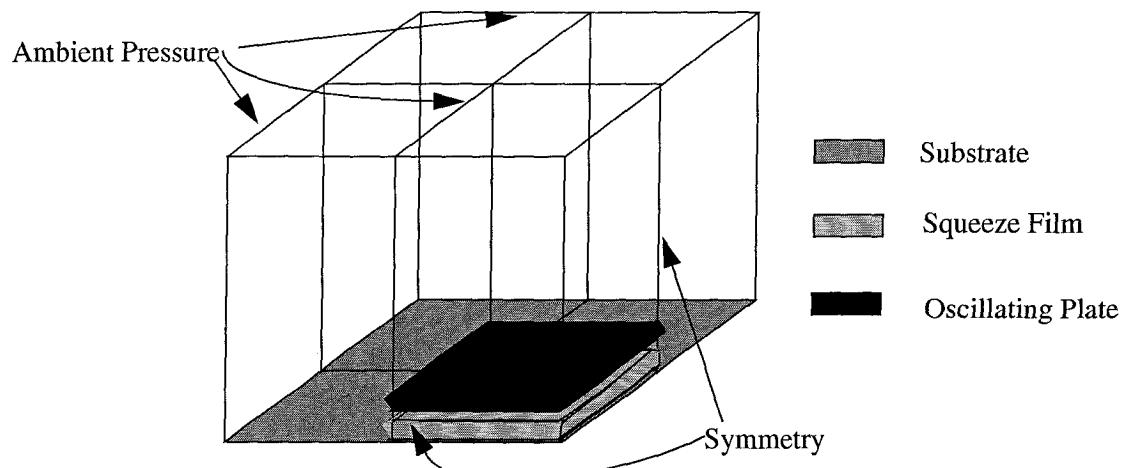
Fig. 2.5 (a): Squeeze film with extended boundary
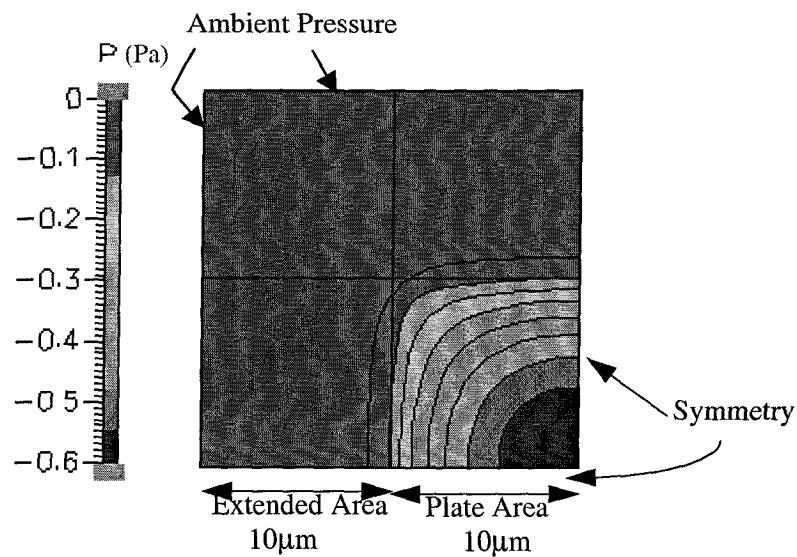
Fig. 2.5 (b): Pressure distribution across and around the top plate (20 μm X 20 μm) oscillating with an amplitude of 0.1 μm at 1 kHz

2.3.2 Non-trivial boundary conditions

The use of non-trivial boundary conditions are more realistic boundary conditions by allowing the solver to arrive at the gauge pressure at the plate edges. This is done by extending the control volume around the oscillating plate and setting the pressure to ambient pressure at the extended control volume boundary. Fig. 2.5 (a) shows the system with non-trivial boundary conditions with blocks of air surrounding the plate oscillating above an infinite substrate. Fig. 2.5 (b) shows the pressure distribution across the quarter plate. Notice that the pressure contours extend beyond the plate edges.

2.3.3 Trivial boundary conditions vs. non-trivial boundary conditions

In practice, the pressure at the plate edges is non-zero. When trivial boundary conditions (TBC) are used, this value is forced to zero and causes underestimation of the gauge pressure distribution across the plate. This results in the underestimation of the damping force due to squeeze action. This problem can be mitigated by the use of non-trivial boundary conditions (NTBC) which models the boundary conditions more realistically.

The following table provides the squeeze force predicted by the use of NTBC and TBC when a plate of varying size oscillates with an amplitude of 0.1 μm and frequency of 1 kHz, 2 μm above the substrate. It can be observed from the table that the difference in force predicted by TBC and NTBC decreases as the plate size increases. This can be intuitively explained because the edge-effects and the finite-size effects decrease with increasing plate size reaching zero for an infinitely large plate. The dominance of the edge and the finite-size effects for sub-100 μm plates has already been experimentally verified in case of lateral viscous damping. For developing behavioral

Plate Size	TBC	NTBC	Difference
20μm	109.1 pN	151.0 pN	27.8%
100μm	62.5 nN	67.1 nN	7.6%
1mm	0.65 mN	0.67 mN	2.9%

models for damping for use in MEMS-scale structures, all finite element simulations are done using non-trivial boundary conditions to take care of the edge and the finite-size effects.

The use of NTBC results in the increase in the number of grid cells from 500 to 5000 as a result of which, a typical transient simulation time increases from 5 minutes in TBC to 60 minutes in NTBC on a 360 MHz Sun Ultra-Sparc. The memory requirements of the simulation is 5 MB in TBC and 45 MB in NTBC. Though there is an increase in the use of computer resources in terms of CPU-time and memory, this provides the solver with more realistic boundary conditions to give accurate results.

2.4 Lumped parameter model

A lumped parameter model consisting of parallel branches of series connected spring and damper elements can be derived to model the damping force given by EQ. 2.4 and EQ. 2.5, with force as the through variable and velocity as the across variable. To derive the values of the spring and the damper elements, we consider the following spring-damper element ladder:

Force F
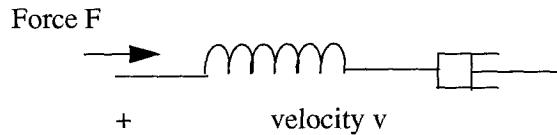
Fig 2.6 A branch with series connected spring and damper elements

The velocity across the terminals of the ladder is the sum of the relative velocities across the spring and the damper elements (EQ. 2.7 and EQ. 2.8). Considering the through variable and the across variable to be vectors of angular frequency ω, the final relation is described in EQ. 2.11.

$$\overline{V} = \overline{V_{spring}} + \overline{V_{damper}} \qquad \text{EQ. 2.8}$$

$$\overline{v} = \frac{\overline{F}}{B} + \frac{d}{dt}\left(\frac{\overline{F}}{k}\right) \qquad \text{EQ. 2.9}$$

$$j\omega \overline{z} = \frac{\overline{F}}{B} + j\omega\left(\frac{\overline{F}}{k}\right) \qquad \text{EQ. 2.10}$$

$$\frac{\overline{F}}{\overline{z}} = \frac{kB^2\omega^2}{k^2 + \omega^2 B^2} + j\frac{Bk^2\omega}{k^2 + \omega^2 B^2} \qquad \text{EQ. 2.11}$$

The real part, in phase with the displacement vector, is the spring component and the imaginary part is the damping component. Upon comparing the imaginary and real parts of EQ. 2.11

with the force terms in EQ. 2.4 and EQ. 2.5 respectively, the values of the spring and the damper

elements is obtained for a given pair of odd integers m, n [7].

$$k_{mn} = \frac{6lwP_a}{(mn)^2 \pi^4 (g+z)}$$

$$B_{mn} = \frac{768(lw)^3 \eta_{eff}}{(mn)^2 (m^2 l^2 + n^2 w^2) \pi^6 (g+z)^3}$$

With the elements as given in the above equations, the lumped parameter model can be repre-

sented as shown in Fig. 2.7. Each series branch represents a pair of spring and damping forces for

a given value of m, n. The number of such branches depends on the required accuracy. The trunca-

tion error can be restricted to under 1% with the use of six branches.
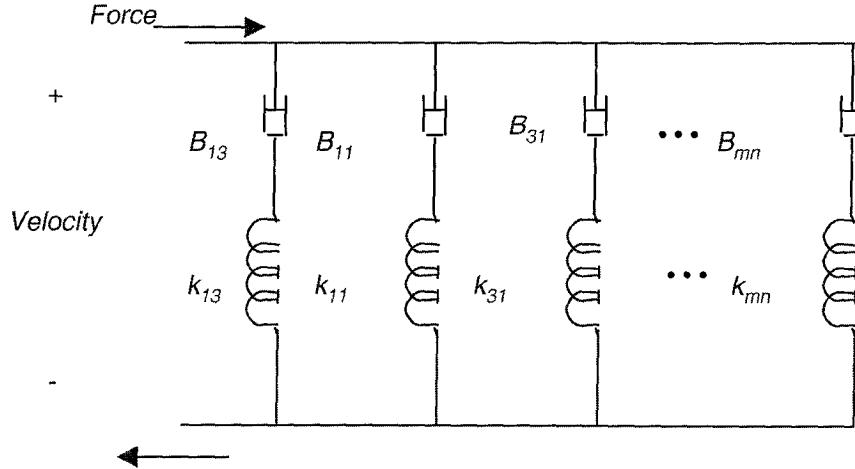
Fig. 2.7: The spring-damper lumped parameter model

This model has been implemented in Verilog-A [8] for use with the node-based MEMS simu-

lation tool developed at Carnegie Mellon University [9, 10]. It has also been implemented in

MAST to be used with a similar library in SABER environment [11]. The model accepts the dis-

placement across the terminals of the model as lumped parameter inputs and uses a voltage con-

trolled voltage source to generate velocity by a differential operator. The sum of the force through

all the parallel branches represents the total damping force. The model is parameterized and can be

used in design. The input parameters are length and width of the plate, gap (the thickness of the

film) and the ambient pressure. The effective viscosity is calculated using Knudsen number which

in turn is evaluated for a given input ambient pressure.

Some equivalent circuit, lumped parameter models for squeeze film damping have been proposed in the past [3, 12]. There are a couple of advantages of representing the model in terms of spring and damper elements rather than circuit elements like resistors, capacitors and inductors [3, 12]. Firstly, the mapping of the through variable (force) and the across variable (position) from the mechanical domain to the electrical domain is not canonical. So is the case with the elements used in the lumped parameter model. For example, the spring element can be modeled by an inductive or a capacitive element while a damping element can be modeled by a resistive or a conductive (both dissipative) element. Secondly, in an integrated MEMS simulation environment, there are different domains (e.g. electrical, mechanical and magnetic domains), each of which has its own through and across variable. If an electrical equivalent circuit model is used to model mechanical damping elements, there arises a need to separate the current which represents the force of mechanical domain from the current that represents the electrical through variable. Hence, ease of use, the use of spring-damper model is helpful.

2.5 Non idealities

2.5.1 Edge and finite-size effects

The force equations EQ. 2.4 and EQ. 2.5 derived from the linearized Reynold's equation do not consider the edge and the finite-size effects. The edge-effects are significant at tens of microns scaled structure as shown in section 2.3. To study the accuracy of the spring-damper lumped parameter model based on EQ. 2.12 and EQ. 2.13, we compare the response of the behavioral model with that of finite-element simulations, for varying squeeze film size. The error in the peak damping force predicted by the behavioral model as compared to FEM simulations for a plate oscillating with an amplitude of 0.1 μm and frequency of 1 kHz is shown in the plot in Fig. 2.8. The degradation in the accuracy of the model at plate sizes in the range of few tens of microns is noticeable. This is because the edge and the finite-size effects become significant at these MEMS-scaled plate sizes.
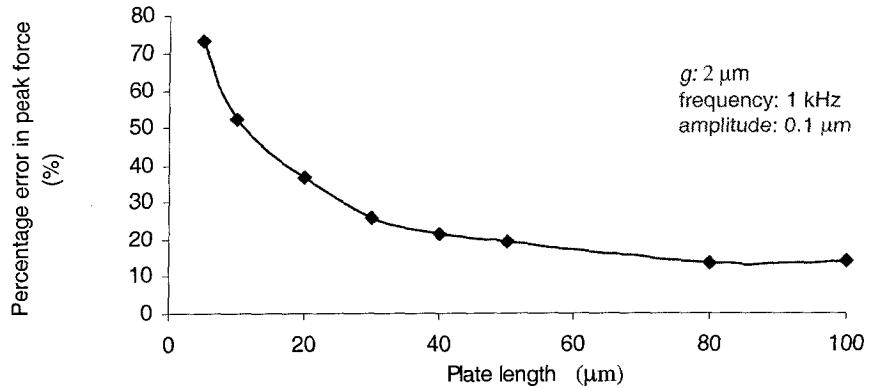
Fig 2.8: Accuracy degradation of the model for small plate sizes

2.5.2 Edge-effect model

There can be several ways in which the edge and the finite-size effects can be modeled. Here we describe a couple of approaches and outline our implementation.

One technique to model the edge effects is the effective viscosity of the model to compensate for the underestimation of the damping force. This approach quantitatively increases the estimated damping force, but does not provide a direct qualitative intuition to model the edge-effects. As effective viscosity is already used to model the slip conditions encountered in narrow gaps, a model of $\eta_{eff} = f(slip, edge)$ will make it difficult for designers to understand which effect is dominant.

Another approach can be to use an effective pressure above the ambient pressure to take care of the non-zero pressure at the plate edges. Pressure is one of the input parameters of the model that is used in the evaluation of the Knudsen number and the effective viscosity. Hence this effect is not distinct from the effective viscosity approach.

There is a need to model the edge effects using parameters that are decoupled from the other parameters. The plate width and length are such independent parameters. Hence, increasing the plate size to account for the non-zero gauge pressure at the plate edges is one straightforward method for modeling the edge effects. This solution is also physically intuitive because the differential pressure becomes zero only at a finite non-zero distance from the plate edge. So extending

gap: 2 μm
Oscillation amplitude: 0.1 μm
Oscillation frequency: 1 kHz
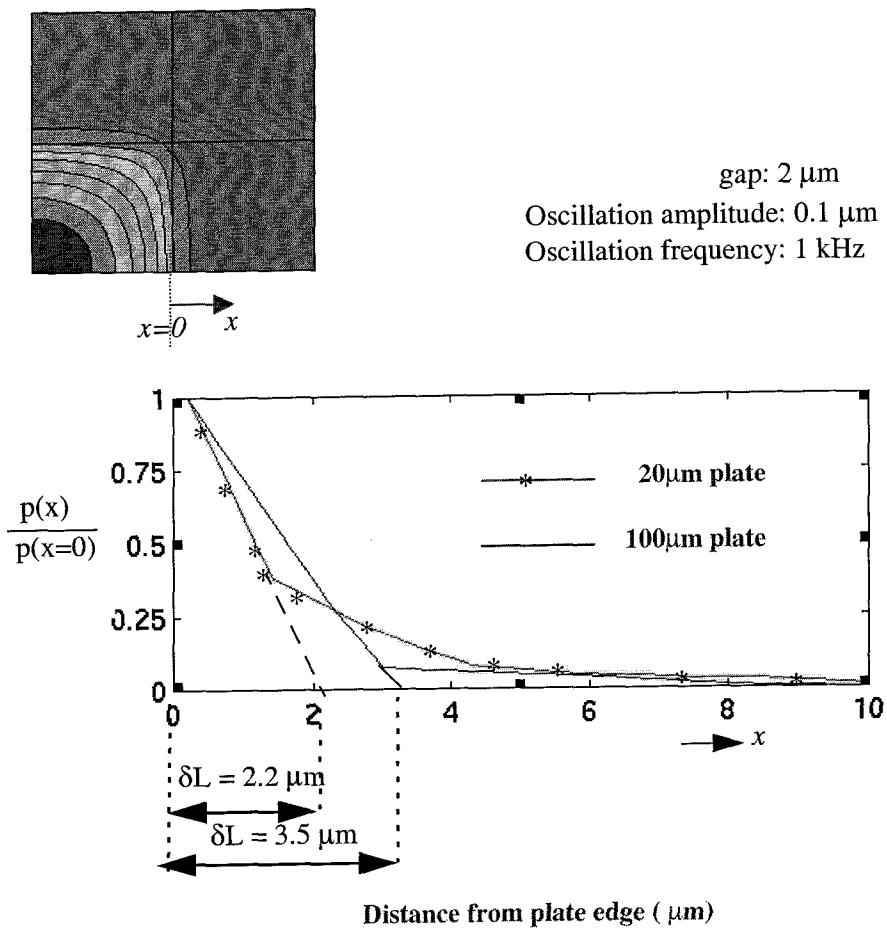
Fig. 2.9: Pressure distribution beyond the plate edge

the plate edge and using trivial boundary conditions at the extended edge provide a way of obtaining more realistic pressure distribution across the plate. Fig. 2.9 shows the pressure distribution and decay beyond the plate edges when the top plate is moving sinusoidally with an amplitude of 0.1 μm and frequency of 1kHz.

The non-zero pressure distribution along the original plate edge is accounted for by extending the plate edge by an amount δL and using TBC at the extended edge [7].

The value of δL shown in the Fig. 2.9 illustrates the physical intuition behind the solution adopted. The quantitative equation for the plate extension is obtained by comparing the peak damping force of the original behavioral model with that from FEA. The parameters that can affect δL are identified as the gap, plate dimensions, frequency of oscillation and the amplitude of oscil-
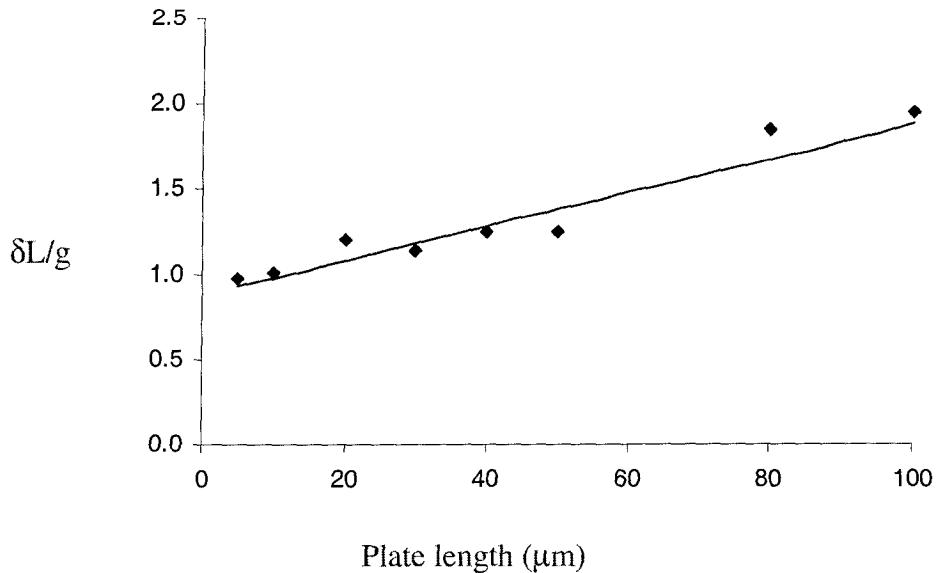
Fig. 2.10: Linear fit with least sum of squared errors for square plates oscillating with
frequency of 1kHz and an amplitude of 0.1 μm

lation. Screening experiments were performed to find the dependency of δL on these factors by

varying these parameters one at a time. All experiments were performed for square plates. The

plate size was varied from 5 μm to 100 μm, gap size from 1 μm to 5 μm and the frequency up to 1

MHz. The amplitude of oscillation was kept under 10% of the gap. For above mentioned plate

sizes and gaps, the value of δL that gives the closest match between the behavioral and finite ele-

ment results was determined. δL has a first-order dependency on the gap and a second-order

dependency on the plate size. Fig. 2.10 shows the plot of δL/g as a function of the plate size.

Larger plates cause more pressure perturbation at the plate edge and the pressure settles to ambient

pressure further away from the edge. Hence, larger plates require a higher value of δL.

The best fit model for δL is given by EQ. 2.14.

$$\delta L(g, L) = g(0.8792 + 0.1L)$$ EQ. 2.14

where L is the plate dimension in microns, g is the gap and δL is the extension.

When the value of gap is decreased, we would expect the squeeze force to increase as the con-

tinuum squeeze action is proportional to $1/g^3$ This can lead to the conclusion that δL should

increase when the gap is decreased. On the contrary, the equation shows that δL is directly propor-

tional to the gap. To understand this, we need to consider the regime of operation. We can consider

the air to be within the continuum limits when the Knudsen number is << 1 (<0.01). The molecular

mean free path of air at standard temperature and pressure is 0.07 μm. So for gaps < 7 μm, the continuum limits are no longer valid. Slip conditions begin to occur. In such conditions, the edge

effects increase with increasing gap and hence δL is directly proportional to gap.

2.5.3 Extended model

The accuracy of the model can be extended by modeling the edge and the finite size effects.

The width w, and the length l of the squeeze film are increased by δL to give the effective width

w_{eff} and effective length l_{eff} as in EQ.2.15 and EQ. 2.16.

$$W_{eff} = w + \delta L(g,w)$$ EQ. 2.15

$$l_{eff} = l + \delta L(g,l)$$ EQ. 2.16

The values of the spring and the damper elements in the extended model is given by substituting w_{eff} and l_{eff} for w and l respectively in EQ. 2.12 and EQ. 2.13. Upon extending the plate dimensions, the improved accuracy of the model is shown in the plot in Fig. 2.11. The accuracy is within

5% for plate sizes in the range of 5 μm to 100 μm.
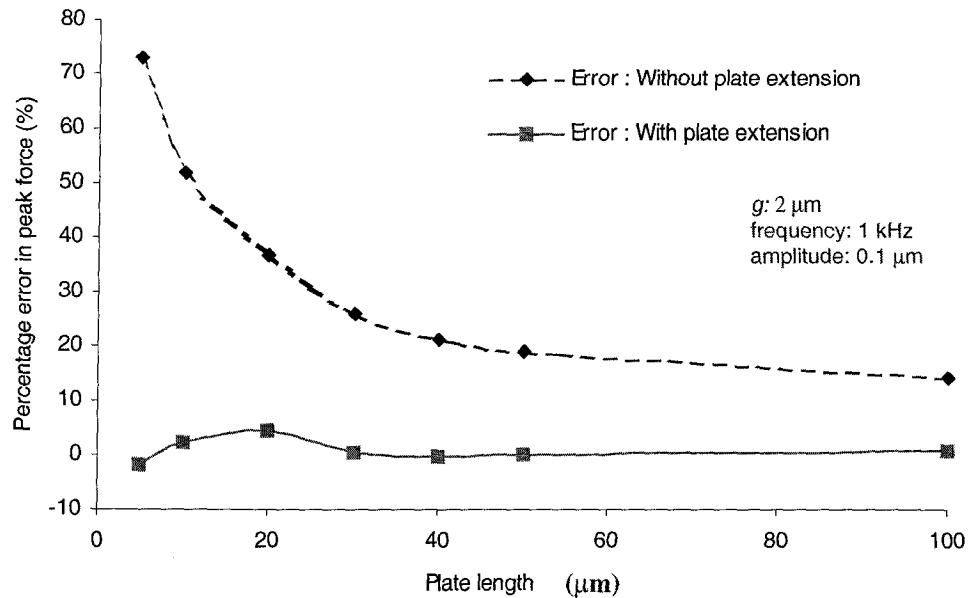
Fig. 2.11: Improved accuracy of the model with extended edges of square plates

2.6 Squeeze film simulation results

In this section, squeeze film simulation results using the extended lumped parameter model described in section 2.5 are discussed. Simulation results for the input of three dominant harmonics of a square wave are presented. Behavioral and finite element simulations are compared for varying aspect ratio of the plate, amplitude of motion and frequency of oscillation. A system level simulation of a resonator bandpass filter having squeeze film damping as the dominant source of energy dissipation is presented. Simulation results are validated experimentally.

2.6.1 Step function response

The squeeze film model has been derived under the assumption of sinusoidal oscillations of the top plate. To study the accuracy of the model for non-sinusoidal input displacement, behavioral simulations with the first three harmonics of a square wave are performed and the results compared to the finite element simulations. Fig 2.12 shows the displacement of the top plate which is the sum of the three dominant harmonics of a square wave of amplitude 0.1 μm and a frequency of 10 kHz. The force on an 100 μm square plate, with a gap of 2 μm and 4 μm, as a function of time is plotted in Fig. 2.13 (a) and Fig. 2.13 (b) respectively. The difference in peak force is under 1% in the case of the 2 μm gap and 15% in the case of the 4 μm gap.

2.6.2 Aspect ratio dependency

While deriving the finite size and the edge-effect model and determining the accuracy of the model in the section 2.5, square plates were considered. The effect of aspect ratio on squeeze film damping is studied by keeping the area constant and changing the length to width ratio of the squeeze film. Damping force on a plate of area 10000 μm^2 is determined for aspect ratios in the range of 1-10. As the aspect ratio increases, as expected, the squeeze action decreases because air underneath the plate with higher length to width ratio can flow out without much squeeze action. Fig. 2.14 shows that the behavioral simulations match the finite element simulations to within 7%. This validates the edge effect model for higher aspect ratios, even though the model was derived with square plates.
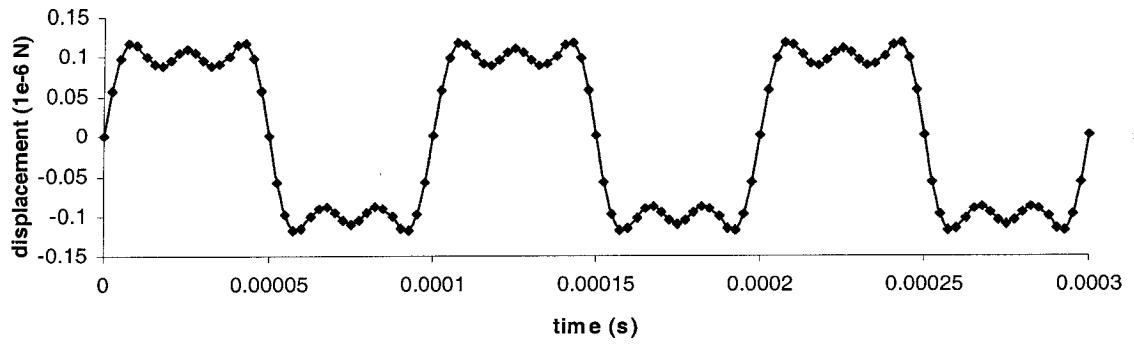
Fig 2.12: Displacement of the top plate with three dominant harmonics of a square wave
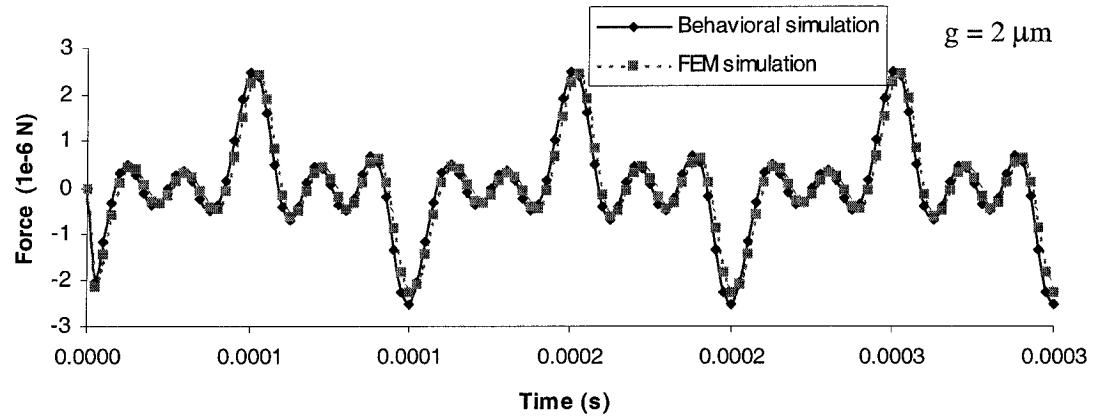
Fig. 2.13 (a): Force on a 100 μm square plate with gap of 2 μm
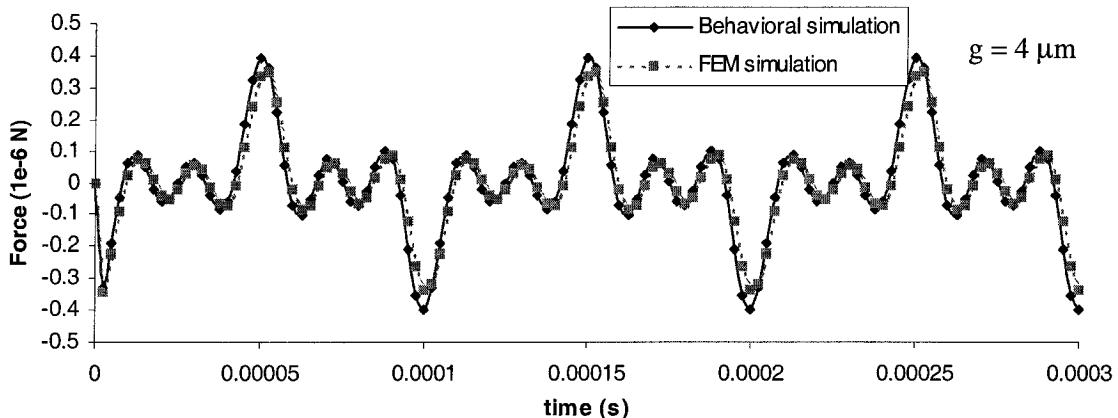
Fig. 2.13 (b): Force on a 100 μm square plate with gap of 4 μm

2.6.3 Amplitude of motion

The damping model consists of non-linear spring and damper elements. Thus, the damping force is not linearly proportional to the displacement. However, for displacements that are small compared to the gap (<10%), the model behaves close to a linear system.
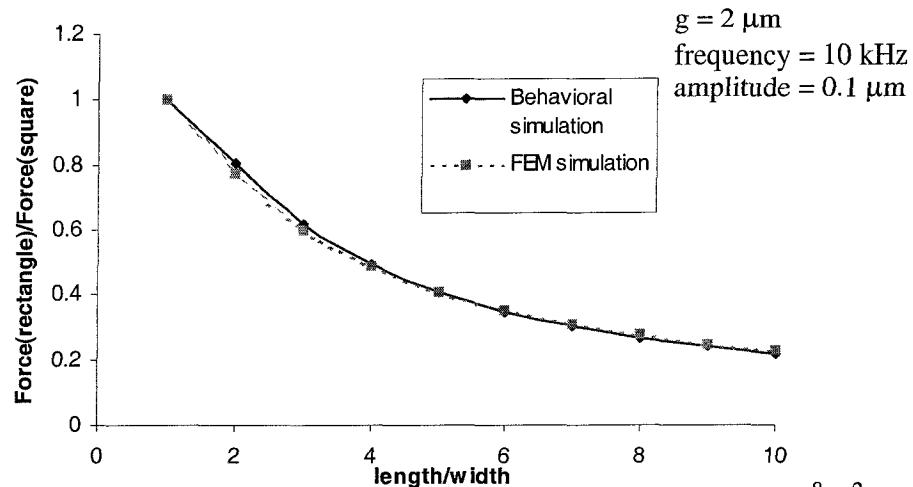
Fig. 2.14 (a): Ratio of force on rectangular plate to that on square plate for a 10^{-8} m^2 area
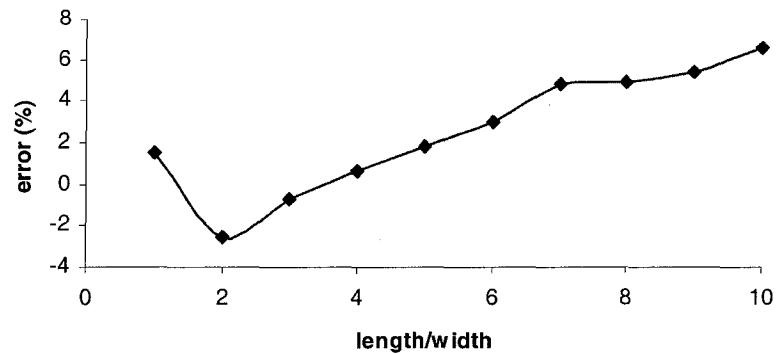
Fig. 2.14 (b): Error in peak force when compared to FEM simulations

The peak damping force for a 10 kHz sinusoidal input of amplitude varying from 40 nm to 200 nm is shown in Fig. 2.15 (a) - Fig. 2.15 (d) for square plates of size 20 μm and 100 μm, and gaps of 2μm, 4 μm. The error, as compared to the numerical simulations is within 10% for all the four cases. The plot shows the linearity of the system decreases with increasing gap.

2.6.4 Frequency dependency

Frequency of the plate oscillations is an important parameter in determining the squeeze force. When the plate oscillates with low frequency, the air flow is nearly incompressible. In such cases, the damping force that is proportional to the velocity dominates the spring force. The total squeeze force is proportional to the frequency for a given amplitude of motion and for fixed phys-
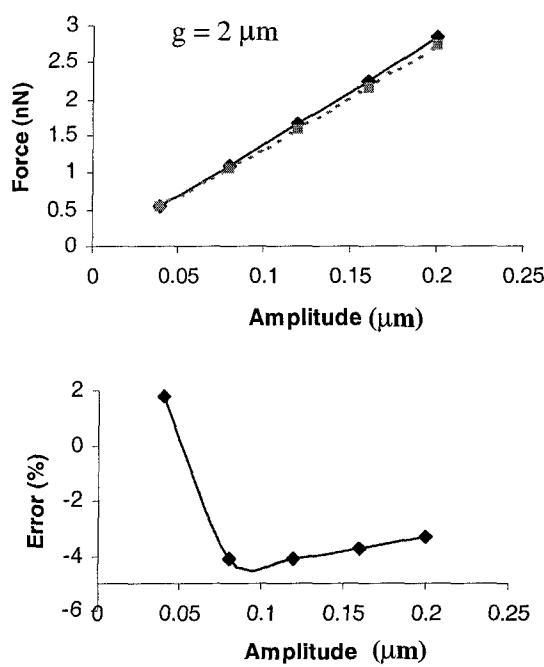
Fig. 2.15 (a): Force and error for a 20 μm square plate and 2 μm gap
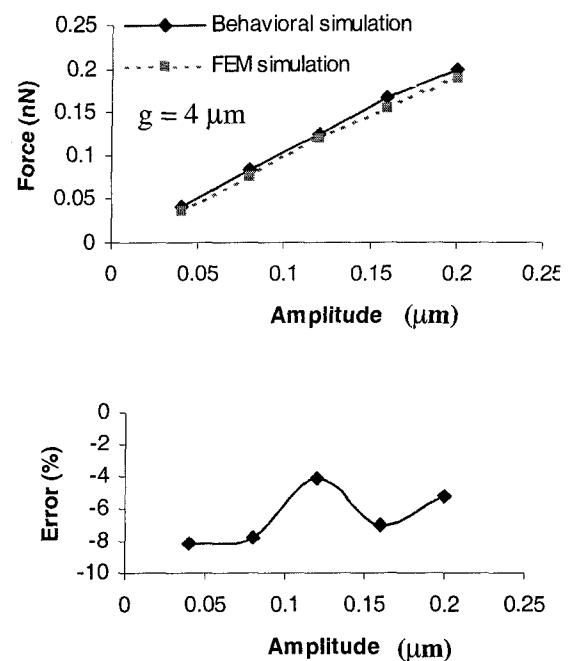
Fig. 2.15 (b): Force and error for a 20 μm square plate and 4 μm gap
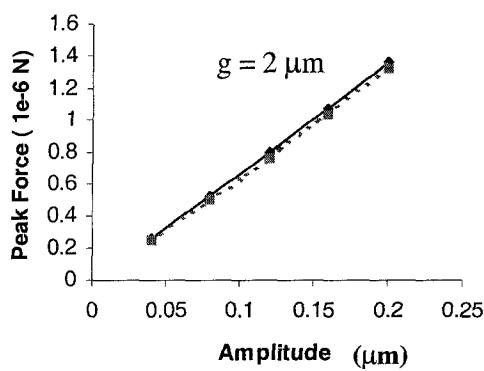
Fig. 2.15 (c): Force and error for 100 μm square plate and 2 μm gap
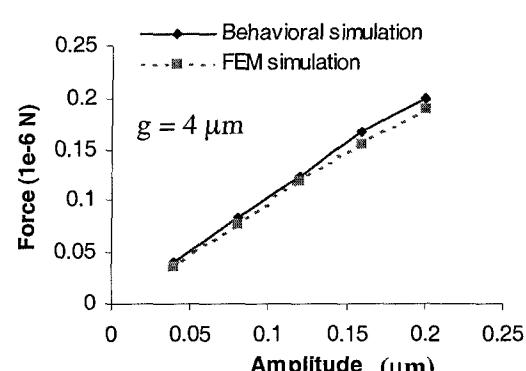
Fig 2.15 (d): Force and error for 100 μm square plate and 4 μm gap
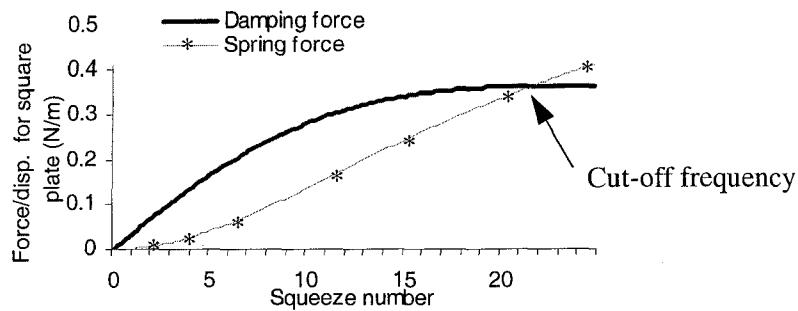
Fig 2.16: Spring and damping forces per unit displacement as a function of squeeze number
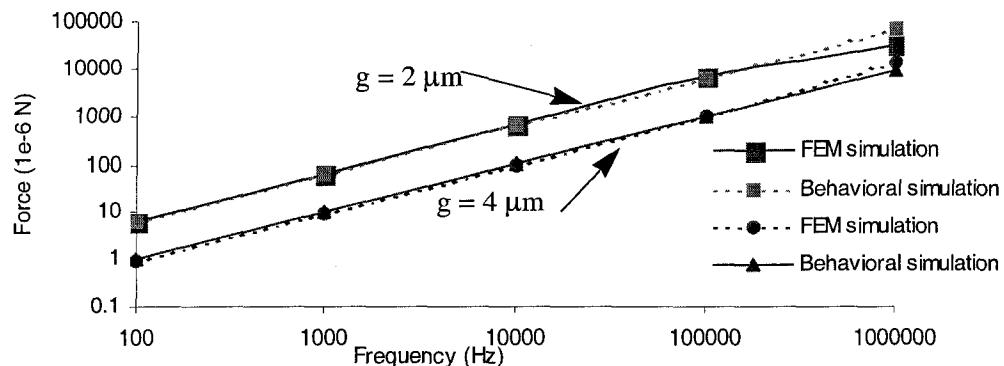
Fig. 2.17: Peak force for different frequencies for a 100 μm square plate
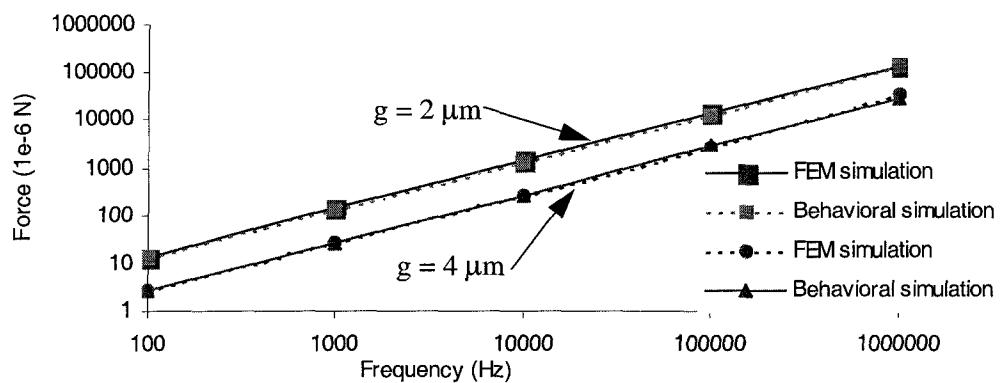
Fig. 2.18: Peak force for a 20 μm square plate

ical dimensions of the squeeze film. At high frequencies, the flow invoked becomes compressible. As a result, the inertial effects of the fluid contribute to the damping. The relative contribution of the spring and the damping terms is plotted as a function of squeeze number (EQ. 2.7) in Fig. 2.16. Cut-off frequency is defined as the frequency at which the spring and the damping terms contribute equally. At frequencies comparable to and higher than the cut-off frequency, the inertial effects

are significant. As a result, the gauge pressure is not negligible compared to the ambient pressure contradicting one of the assumptions in the squeeze film model [1]. Hence the error at the high frequencies can be significant. Fig. 2.17 plots the peak force as a function of frequency for the case of a 100 μm square plate with gaps of 2 μm and 4 μm. For the gap of 2 μm, cut-off frequency for an 100 μm square plate is 670 kHz. From FEM simulations, the peak gauge pressure at 1 MHz is as high as 12 kPa. This is about 12% of the ambient pressure (0.1 MPa). The assumption of small gauge pressure fails resulting in the high error noticeable at frequencies close to 1 MHz. The error in peak damping force for a gap of 2 μm is about 50% while it is 29% for a gap of 4μm. This can be attributed to decrease in the squeeze number with the increase in gap. Fig. 2.18 plots the peak force for a 20 μm square plate. Accuracy is within 10% in this case as cut-off frequency is 16 MHz for g =2 μm.

3. Lateral viscous damping

3.1 Introduction

Viscous lateral damping, also known as slide film damping, occurs when two parallel plates are in relative tangential motion. The relative motion of the parallel structures invokes a fluid flow that exerts a force opposing the relative motion. The force exerted by this mechanism depends on the velocity gradient of the fluid near the plane of the oscillating structure, the viscosity of the medium and the area of the oscillating structure. The velocity gradient of the fluid in turn depends on the velocity of the oscillating plate, and its distance from other parallel structures that are in relative motion. Hence a slide film between two parallel plates is characterized by the length and the width of the plates, the distance between them, their relative velocity and the viscosity of the film.

Viscous damping is a dominant source of energy dissipation in laterally-driven microstructures. A lateral resonator is a common example. The proofmass oscillating parallel to a substrate experiences viscous drag by fluid both on the top and the bottom surfaces. In lateral comb drives, lateral damping can be a dominant source of damping. There are four different lateral damping sources in a lateral comb drive. Between the stator and the rotor fingers, there are two slide films associated with each rotor finger (one on each side of the rotor finger) as in Fig. 3.1 (a). These films are characterized by the overlap length of the stator and the rotor fingers, the thickness of the fingers and the equilibrium distance between the fingers. There is additional damping from the fluid above and below the rotor finger. This damping source acts on the entire rotor area as shown in Fig. 3.1 (b). The bottom film is characterized by the distance from the substrate and the top film can be infinitely thick if exposed to atmosphere.

Slide film
Rotor finger
Rotor truss
Stator
Substrate
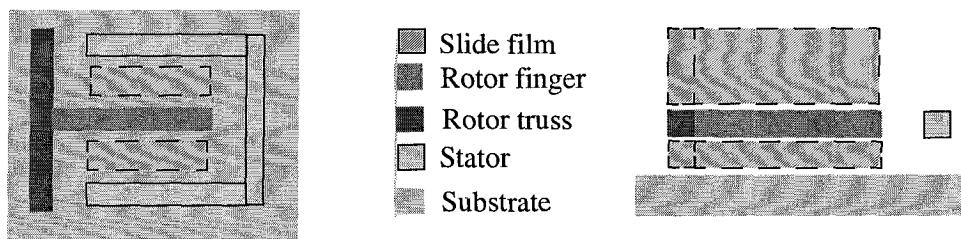
(a) Top view showing the slide films
between the stator and rotor fingers

(b) Cross section showing the slide films
on the top and bottom of the rotor

Fig. 3.1: Slide films in a lateral comb drive

3.2 Slide film model

3.2.1 Model for continuum conditions

The oscillations of a planar structure in a gaseous medium invoke flow in the surrounding medium. This section describes the theoretical aspects and the way the invoked flow is modeled. Consider a plate in the X-Y plane oscillating in the X-direction. The dynamics of the gas flow invoked can be modeled by the one-dimensional diffusion equation (EQ. 3.1) [13, 14].

$$\frac{\partial v(z)}{\partial t} = \mu \frac{\partial^2 v(z)}{\partial z^2} \qquad \text{EQ. 3.1}$$

where μ is the kinematic viscosity of the gas and $v(z)$ is the gas velocity component in the x direction. The kinematic viscosity is the ratio η/ρ where η is the viscosity coefficient or the dynamic viscosity of the gas and ρ is the density of the gas..
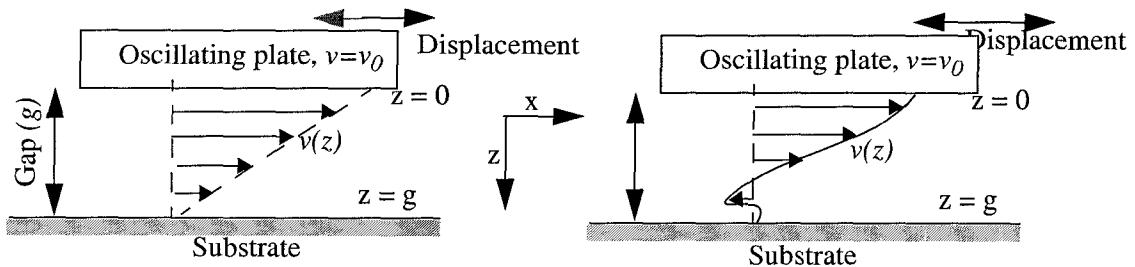
Fig. 3.2: Slide film between a planar oscillating structure and the substrate

For a fully established flow without any transient consideration, the flow can be considered to Couette flow with a linear velocity profile as in Fig. 3.2 (a). There are no inertial effects in this steady state (established) flow. If the continuum limits are considered, the velocity of the gas at the plate surface is equal to the velocity of the plate. Under these conditions, the damping coefficient is given by [13, 14]. :

$$B = \frac{\eta A}{g} \qquad \text{EQ. 3.2}$$

where A is the area of the moving plate and g is the thickness of the slide film.

Couette damping model does not take inertial effects into consideration and hence can be inaccurate at high frequencies. The frequency dependent Stokes flow model takes into account the inertial effects. For a plate velocity of $v_0\cos(\omega t)$, the velocity profile in Stokes flow decays expo-

nentially as shown in Fig. 3.2 (b) and the phase shift varies linearly as we move away from the plate. Under continuum assumptions, the gas velocity profile and the damping are given in EQ. 3.3 and EQ. 3.4.

$$v(z) = -v_0 \frac{sinh(qg - qz)}{sinh(qg)}$$

EQ. 3.3

$$\bar{\xi} = \eta Aq coth(qg)$$

EQ. 3.4

where q is the complex frequency variable given by $(j\omega/\mu)^{1/2}$, ω is the oscillation frequency and μ is the kinetic viscosity and ξ is the complex damping coefficient. A complex damping coefficient means that there is a damping force (the real part) and there is a spring force in phase with the displacement (the imaginary part). As the frequency tends to zero, the Stokes damping model approaches the Couette damping model. The amplitude of the velocity profile decays by a factor of e over a distance equal to the penetration depth δ given by $(\omega/(2\mu))^{1/2}$.

3.2.2 Gas rarefaction effects

Since the critical film dimension, the gap between the two plates, is in the range of microns, the mean free path is comparable to the gap. This causes the gas rarefaction effect, which can be modeled with an effective viscosity. EQ. 3.5 gives the value of effective kinematic viscosity, μ_{eff} and effective dynamic viscosity, η_{eff} [14].

$$\mu_{eff} = \frac{\mu}{1 + 2K_n} \qquad \eta_{eff} = \frac{\eta}{1 + 2K_n}$$

EQ. 3.5
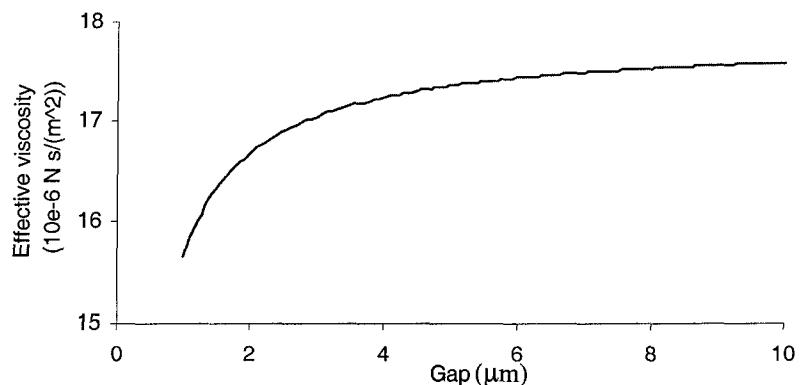
Fig. 3.3: Effective kinematic viscosity as a function of gap

where K_n is the Knudsen number which is the ratio of the mean free path of the gas molecules to the distance between the plates. Fig. 3.3 plots the effective kinematic viscosity of air at standard pressure and temperature, as a function of the plate distance.

The gas velocity at the plate surface is not the same as the plate velocity due to gas rarefaction. Slip conditions occur and the velocities at the plate and substrate surfaces, which are the boundary conditions for EQ. 3.1, are given in EQ. 3.6 and EQ. 3.7 [14].

$$v(0) = v_0 + \lambda \frac{\partial v(z)}{\partial z}\bigg|_{z=0} \qquad \text{EQ. 3.6}$$

$$v(g) = -\lambda \frac{\partial v(z)}{\partial z}\bigg|_{z=g} \qquad \text{EQ. 3.7}$$

where v_0 is the plate velocity, λ is the molecular mean free path of air and g is the gap between the plate and the substrate.

3.2.3 Solution for the velocity profile with gas rarefaction

For sinusoidal oscillations of the plate, the solution to EQ. 3.1 with boundary conditions as in EQ. 3.6 and EQ. 3.7 is given as [14]:

$$v(z) = -v_0 \frac{\sinh(qg - qz) + q\lambda \cosh(qg - qz)}{(1 + q^2 \lambda^2)\sinh(qg) + 2q\lambda \cosh(qg)} \qquad \text{EQ. 3.8}$$

From the velocity profile, the damping coefficient ξ can be extracted as in EQ. 3.8.

$$\bar{\xi} = \frac{\eta_{\text{eff}} A}{v_0} \frac{\partial v(z)}{\partial z}\bigg|_{z=0} = \eta_{\text{eff}} Aq \frac{\cosh(qg) + q\lambda \sinh(qg)}{(1 + q^2 \lambda^2)\sinh(qg) + 2q\lambda \cosh(qg)} \qquad \text{EQ. 3.9}$$

where η is the viscosity coefficient (also called dynamic viscosity), A is the area of the plate surface. Gas rarefaction effects are taken into account by using μ_{eff} and η_{eff} for μ and η respectively as in equation 3.5.

As the frequency of oscillation tends to zero, the damping force tends to that of Couette damping force. For very high frequencies, this model tends to Couette damping model with a gap equal to the molecular mean free path of air (λ).
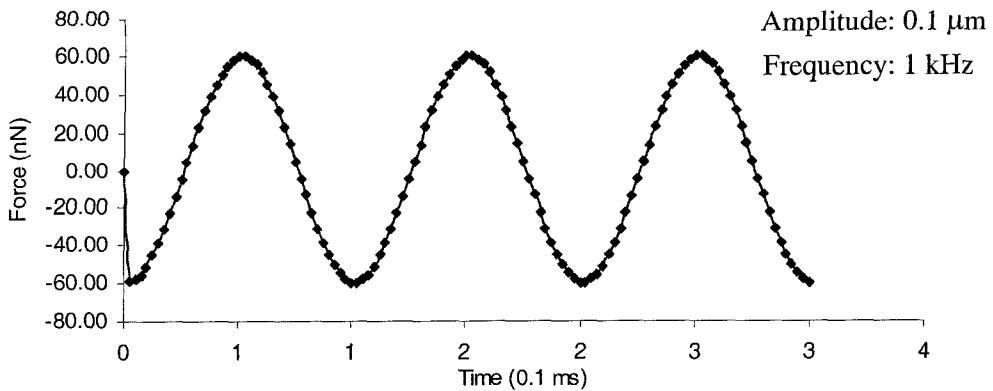
Fig. 3.4: Lateral damping force on a sinusoidally oscillating plate

3.3 Finite element simulation of slide films

FEM simulations to evaluate the lateral damping force on a plate oscillating laterally above an infinite substrate were performed. To verify the finite element simulations being performed, the force on a square plate of size 1mm on a side, oscillating with an amplitude of 0.1 μm and a frequency of 10 kHz was determined. Fig 3.4 shows the damping force with time for a gap of 2 μm. The damping coefficient can be extracted from the peak force. Since the gap is small compared to the penetration depth at 10 kHz, Couette model with linear air velocity profile between the plate and the substrate can be used to evaluate the damping coefficient as in EQ. 3.10 [14].

$$B = \frac{\eta_{eff} A}{g}$$

EQ. 3.10

where g is the gap between the plates, A is the area of the oscillating plate and η_{eff} is the effective dynamic viscosity of air.
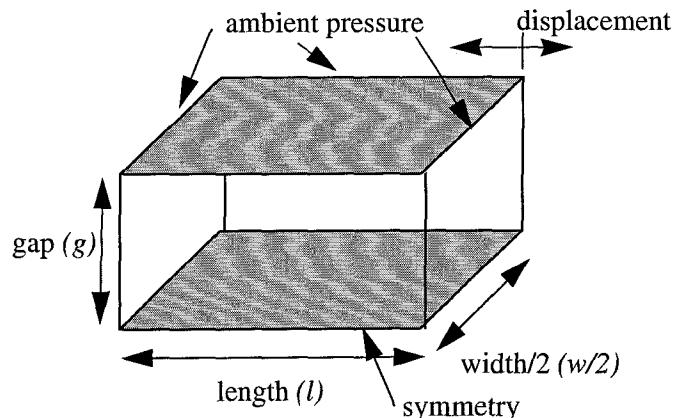

Fig. 3.5: Trivial boundary conditions in finite element simulation of slide film damping

The values of damping coefficient obtained from the FEA method and the analytical method are 9.5 μNs/m and 9.84 μNs/m respectively. They match to within 4% which verifies and quantifies the accuracy of the finite simulations.

As in the case of squeeze film, the type of boundary conditions used affect the accuracy of the finite simulations. The use of trivial and non-trivial boundary conditions in the simulations of lateral damping and the advantages of each approach are discussed next.

3.3.1 Trivial boundary conditions

In trivial boundary conditions (TBC), the slide film is represented by a 3-D structured block enclosed between two wall surfaces and the edges of the wall surfaces are fixed at ambient pressure. The representation does not consider the finite non-zero thickness of the plate. To exploit the symmetry conditions for efficient simulation, one half of the plate is used as shown in Fig. 3.5.

3.3.2 Non-trivial boundary conditions

The use of non-trivial boundary conditions (NTBC) provide the solver with the freedom of evaluating the pressure and hence the air flow around the oscillating structure. The oscillating plate is surrounded by blocks of air on all directions and the ambient pressure boundary conditions
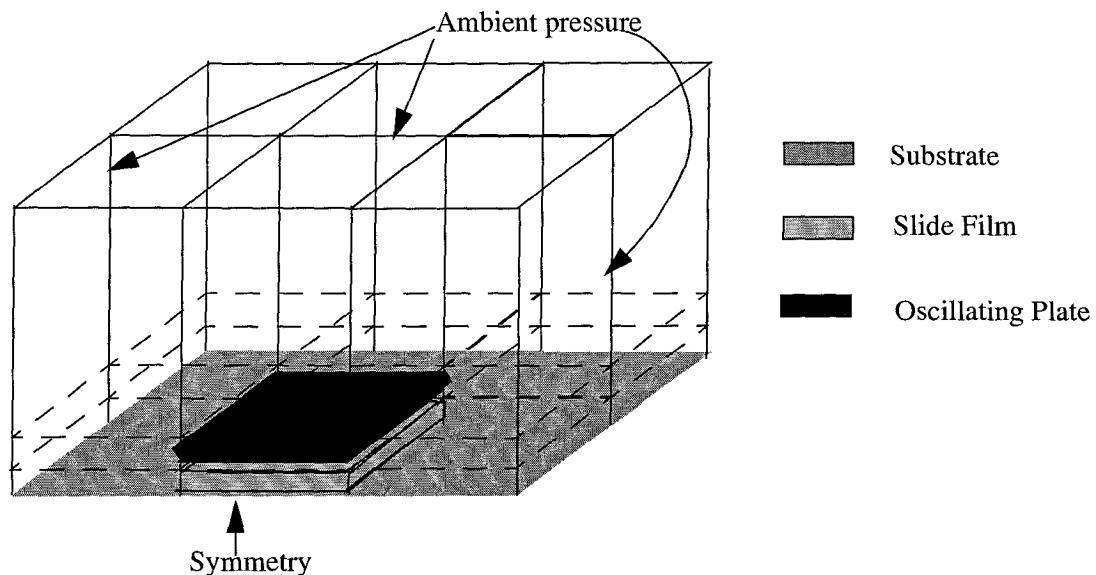

Fig. 3.6: Use of non-trivial boundary conditions in slide film damping

are set at the extended boundaries to model more realistic conditions. Fig. 3.6 shows the system used for the finite element simulations with NTBC

3.3.3 Trivial boundary conditions vs. non-trivial boundary conditions

The following table provides the lateral damping force predicted by the use of NTBC and TBC when a plate of varying size oscillates with an amplitude of 0.1 µm and frequency of 10 kHz, 2 µm above the substrate. It can be observed from the table that the difference in force predicted by TBC, NTBC and the Couette damping model decreases as the plate size increases. The dominance of the edge and the finite-size effects for sizes less than 100 µm on a side has been experimentally observed by Zhang *et al.* [15].

Plate Size	Theoretical (Couette damping)	TBC	NTBC
20um	$0.0597 \ \mu N/m^2$	$0.065 \ \mu N/m^2$	$0.0727 \ \mu N/m^2$
100um	$0.0597 \ \mu N/m^2$	$0.0597 \ \mu N/m^2$	$0.064 \ \mu N/m^2$
1mm	$0.0597 \ \mu N/m^2$	$0.0597 \ \mu N/m^2$	$0.060 \ \mu N/m^2$

As in the case of squeeze film damping, the force is underestimated when TBC are used. This is mitigated by the use of NTBC, but at the expense of additional computer resources. The use of NTBC results in the increase in the number of grid cells from 100 to 4000 as a result of which, a typical transient simulation time increases from 4 minutes in TBC to 45 minutes in NTBC on a 360 MHz Sun Ultra-Sparc machine. The memory requirements of the simulation is 5 MB in TBC and 45 MB in NTBC. Non-trivial boundary conditions are used for all the simulations used to characterize behavioral model.

3.4 Lumped parameter model

The numerator and the denominator of the complex damping coefficient (EQ. 3.9) can be represented by a Taylor series in variable q about the dc value of q (q=0) as in EQ. 3.11. The ratio has

only even powers of q in both the numerator and the denominator which makes it a ratio of complex power series in angular frequency.

$$\bar{\xi} = \frac{\sum\limits_{\substack{i=0 \\ even}}^{\infty} n_i q^i}{\sum\limits_{\substack{i=0 \\ even}}^{\infty} d_i q^i}$$

EQ. 3.11

where n_i are the even coefficients in the numerator and d_i are those in the dominator and are functions of the gap (g) and the mean free path (λ) of air molecules. The equations for the coefficients are given in the appendix.

The condition for the convergence of each series can be set by selecting the ratio of the two successive terms of the real and imaginary parts in each series to be less than unity. Truncation error can be controlled by changing the number of terms in the series and the ratio of successive terms. The minimum ratio of the absolute values of successive terms in the real and the imaginary parts of the numerator and the denominator of EQ. 3.11 is $g^4\omega^2/24\mu^2$. The ratio $g^4\omega^2/24\mu^2$ is kept under 0.1 to truncate the series after first three terms. As an upper bound on the operation frequency for a given g and μ. For example for $g = 2\ \mu m$ and $\mu = 17.9\ \mu Nms/kg$, $\omega < 6.9 \times 10^6\ s^{-1}$.
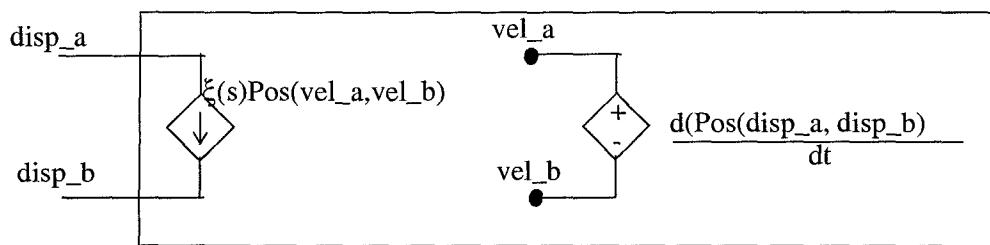
Fig. 3.7: Lateral damping model in Verilog-A

The transfer function described is implemented in Verilog-A as a Laplace transform. The one dimensional slide film model has two pins indicating the displacement of the oscillating plate and the substrate. This is converted into relative velocity using a time derivative operator. This relative velocity is used to compute the damping in the frequency domain and inverse Laplace transform back to damping force between the plate and the substrate. The input parameters of the model
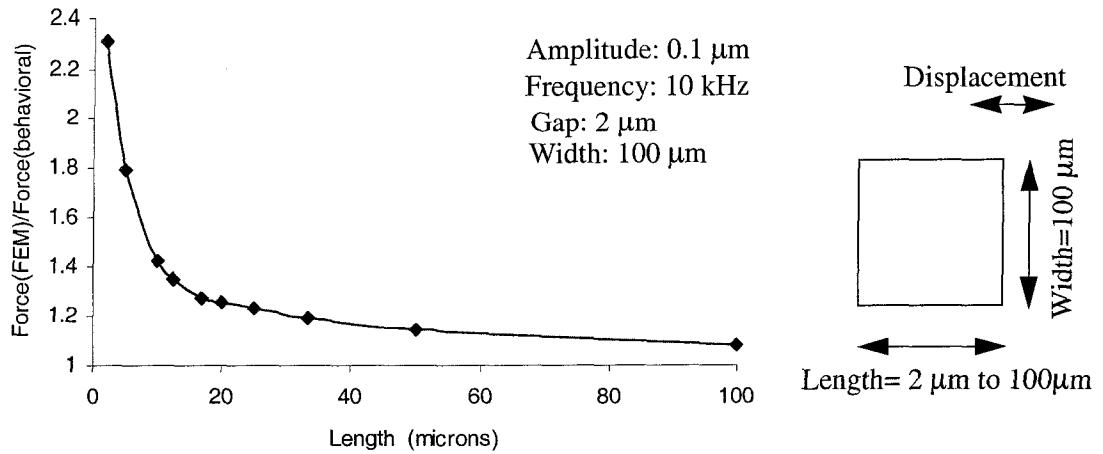
Fig. 3.8: Ratio of peak damping force for varying length

include the length and the width of the plate, the gap and the ambient pressure. Fig. 3.7 shows the circuit implementation of the model.

3.4.1 Edge effects in the lumped parameter model

The damping force given by EQ. 3.9 does not take into account the edge and the finite size effects which are dominant at micron-scale devices. This observation was made experimentally by Zhang. *et al.* and it was suggested that the damping force be multiplied by an empirical correction factor of about 2 to 3 [15]. Since the motion of the plate is in the plane of the structure, the edge effects can show different dependencies on the width and the length. To study this, we keep one dimension constant while varying the other. Let the dimension of the edge along the direction of motion be *l* (length) and that of the perpendicular edge be *w* (width). The length and the width are varied one at a time while keeping the other fixed at 100 μm to quantify the difference in damping force obtained from behavioral and finite elements simulations.

Fig.3.8 plots the ratio of peak forces from lumped parameter and FEM simulations for lengths varying from 2 μm to 100 μm. For *l*=2 μm, the force estimated by behavioral simulation using the model represented by EQ. 3.9 is less by a factor of 2.3 than the force from FEM simulations, given the edge effects contribution due to finite width is negligible. This is in agreement with the empirical factor used by Zhang *et al.* Peak force is a sufficient metric at the frequencies in the range of
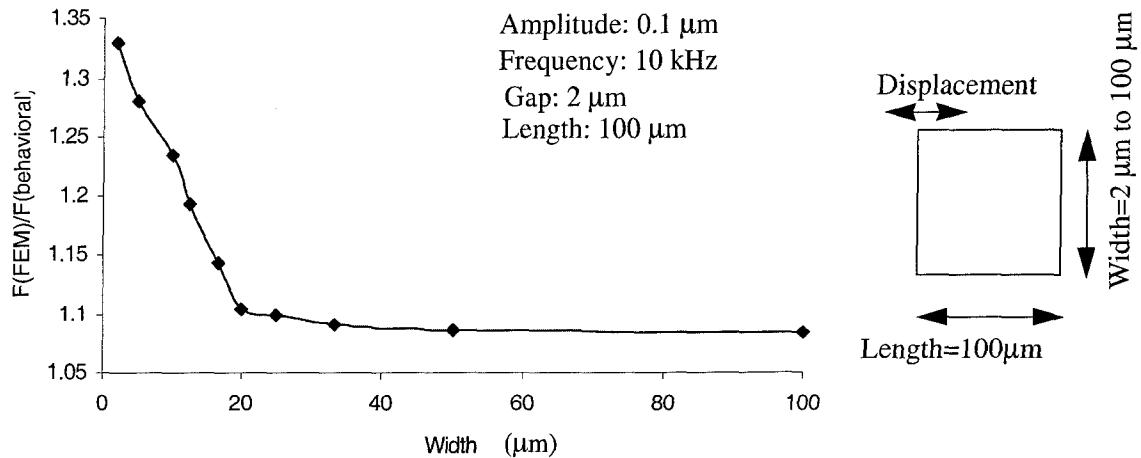
Fig. 3.9: Ratio of peak damping force for varying width

10's of kHz as the damping fore dominates over the spring force and the associated phase difference is less than $1°$.

Fig. 3.9 shows the ratio of peak forces for varying width. The ratio of the forces from behavioral and FEM simulations is about 1.33 for a 2 μm width. This shows that the edge effects depend on the aspect ratio as well as the orientation of the plate.

The contribution of the edge effects is established qualitatively. For quantitative analysis and derivation of the edge effect model, further investigation of the dependencies on gap and the coupled effect of the length and width is required and is left as future work. Further simulations of the lateral damping model will be presented with a fixed plate extension of 4 μm on each side. This translates into a multiplication factor of about 1.08 for a 100 μm square plate which is close to the ratio shown in Fig. 3.8 and 3.9.

3.4.2 Step function response

The damping model used in the derivation of the lumped parameter model was derived for sinusoidal input. To study the response to non-sinusoidal input, a sum of the first three dominant harmonics of a square wave of amplitude 0.1 μm was used as input. Fig. 3.10 are plots of the lateral displacement and force on a 100 μm square, oscillating plate. The plate dimensions were
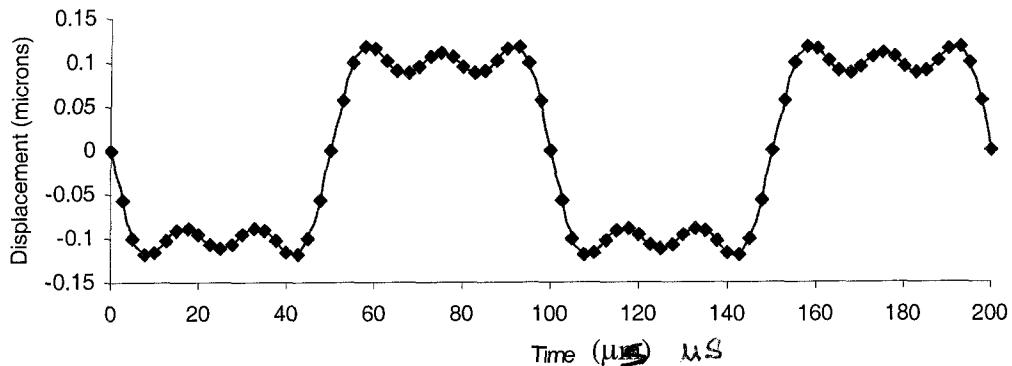
Fig. 3.10 (a): Square wave displacement of the top plate
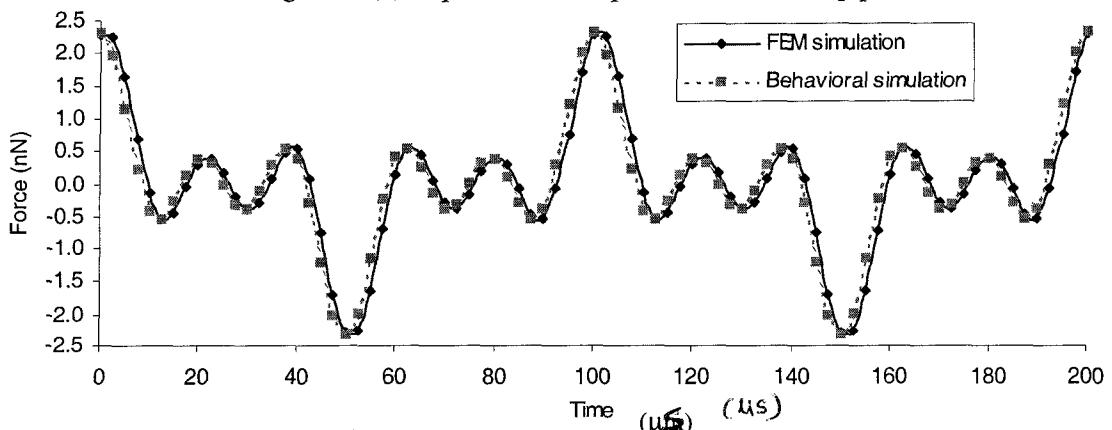
Fig. 3.10 (b): Force for square wave oscillations

extended by 4 μm for which the damping force gets multiplied by a factor of 1.08, which is close to the edge effect ratio in Fig. 3.8 and Fig. 3.9.

3.4.3 Frequency dependency

The lateral damping force is highly frequency dependent. At low frequencies, the fluid near the plate surface can respond to the plate oscillations. In this case, the phase difference between the force and the velocity is zero. Inertial effects are negligible and hence there is no spring component. As the frequency increases, inertial effects come into play and the force on the oscillating plate has both a damping and a spring component. The total force can be analyzed by comparing the amplitude and phase of the force from the behavioral and the FEM simulations. Fig. 3.11 (a) shows the plot of magnitude as a function of frequency on a 100 μm plate. It can be seen that the peak force is almost linear with frequency, at least until 1MHz, after which the amplitude increases more rapidly with increasing frequency. The phase difference between the force and the velocity is plotted in Fig. 3.11 (b). The phase is close to zero for frequencies up to 10 kHz. Phase increases

linearly with frequency. The phase response of the behavioral model matches to within 2° to that

of finite element model for frequencies up to 1 MHz.
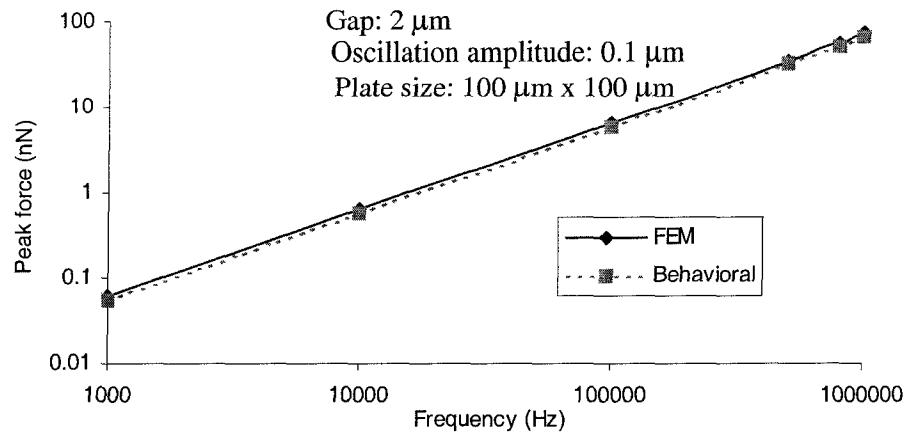
Fig. 3.11 (a): Force amplitude on a 100 μm square plate
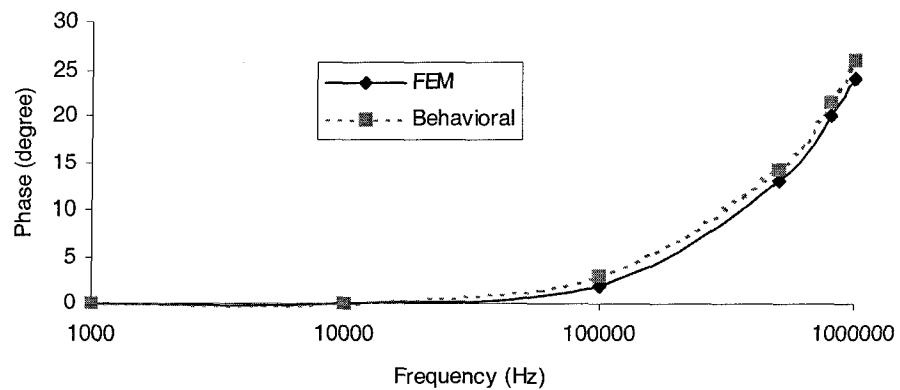
Fig. 3.11 (b): Phase of damping force with respect to velocity

4. System level simulation and experimental verification

This chapter provides the system-level simulation of a bandpass filter and a folded-flexure microresonator. The simulation is done using the NODAS cell library developed at Carnegie Mellon University [9, 10]. The bandpass filter has squeeze film as dominant damping source and the lateral resonator has slide film damping as the dominant source.

4.1 CMOS bandpass resonator filter

To emphasize the use of the behavioral squeeze film model in capturing the dynamics of damping accurately, results of a system level simulation of a bandpass resonator filter are presented and experimentally validated.

Fig. 4.1 shows the schematic diagram of a 550 kHz CMOS micromechanical bandpass filter [16]. The filter is designed using the NODAS parameterized cell library. The filter system is composed of three resonators coupled by "O" springs and is integrated with the associated electrical interface circuitry. Each resonator is designed for a 550 kHz resonance frequency. The system has three resonant peaks scattered around the natural frequency of 550 kHz. The filter consists of three pairs of differential, electrostatic comb drives used for actuation and sensing. The differential comb drives have associated squeeze film damping which is the dominant source of energy dissipation in the comb drives as well as in the resonator filter. The squeeze film between the stator and the rotor fingers has a length of 37 μm, a width of 4.8 μm and a thickness of 1.8 μm. The number of such squeeze films in each comb drive is twice the number of rotor fingers (one on each side of the rotor finger). The lateral damping model used in the simulation is a Couette flow with the gap assumed equal to the penetration depth at 550 kHz.

The output voltage obtained at the sensing comb drive is buffered by the electronics. Fig 4.2 shows the output voltage measured at the output of the interface circuitry. With the use of the damping model with edge effect enhancements, the output voltage at the resonant frequencies matches the experimental measurements to within 0.6 dB, which is equivalent to 7% error in the gain. The results obtained with the use of the behavioral model without any edge extensions differ

Crab-leg spring

Proof mass

Differential combdrive

(a):CMOS resonator

Driving resonator   Coupling resonator   Coupling spring   Sensing resonator

(b): Bandpass resonator filter schematic
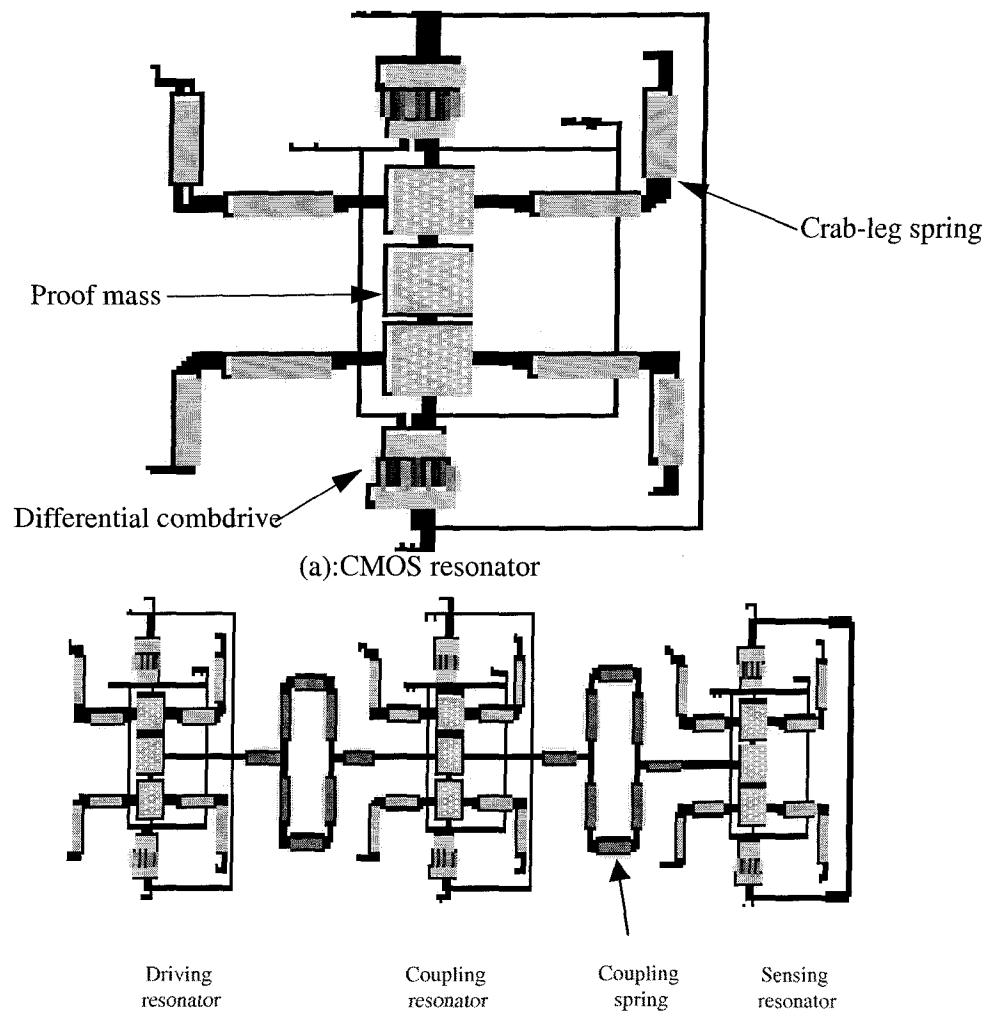
Fig. 4.1: NODAS schematic of the bandpass resonator filter

—————— Experimental

—————— Simulation: With plate extension

- - - - - - Simulation: Without plate extension
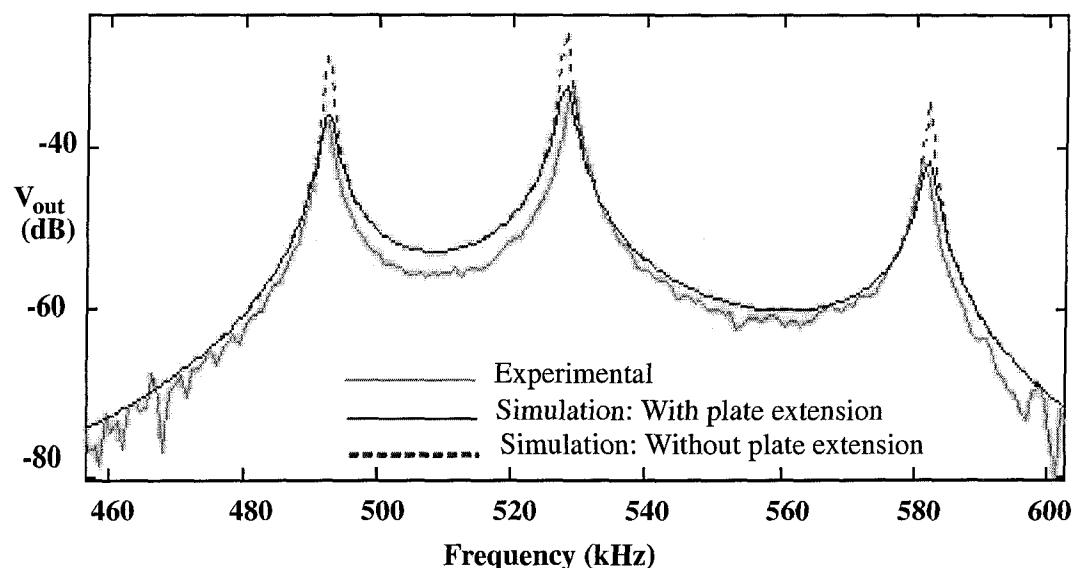
Fig 4.2: AC transfer characteristics of the bandpass filter
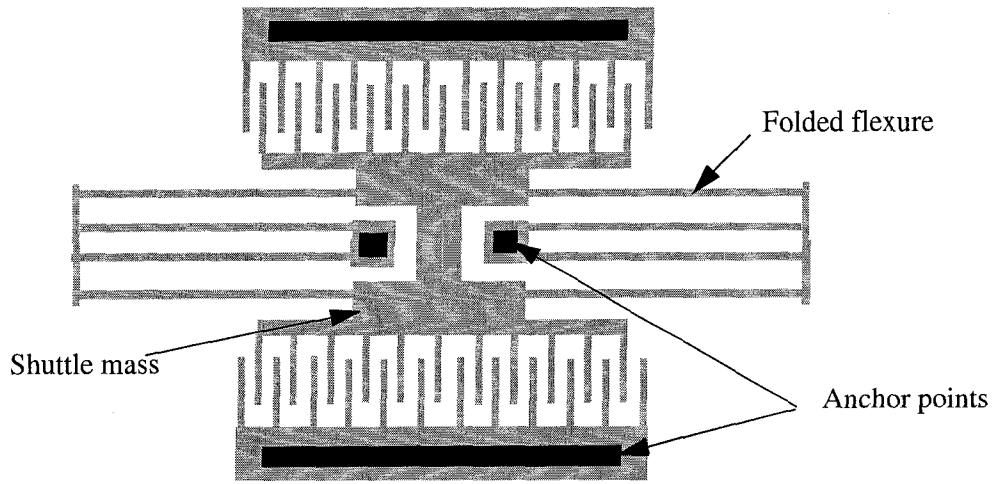
Fig. 4.3. Layout view of the lateral folded-flexure comb-drive microresonator

by 8 dB, a gain error of over 150%.The lateral damping associated with the filter is smaller than the squeeze damping by over an order of magnitude.

4.2 Lateral microresonator

In a lateral microresonator, the lateral slide film damping can be a dominant energy dissipation mechanism. Fig. 4.2 shows the layout view of a folded-flexure lateral resonator [17]. The system can be modeled by a mass-damper-spring system characterized by a resonant frequency and quality factor.

The slide films associated with the all the moving components like the comb drive, the beams and the shuttle mass have associated slide film damping contributing to energy dissipation in the system. Different slide films in the comb drive include the films between the stator and the rotor fingers and between the rotor and the substrate. A detailed description of these is provided in section 3.1. At frequencies less than 100 kHz, the damping force on the bottom surface of the microstructure dominates as the distance between the substrate and the structure (2 μm) is much less than the penetration depth. At frequencies close to or greater than 100 kHz, the penetration depth of air becomes less than 10 μm. Under such conditions, the damping force on the top surface contributes significantly to the overall damping.
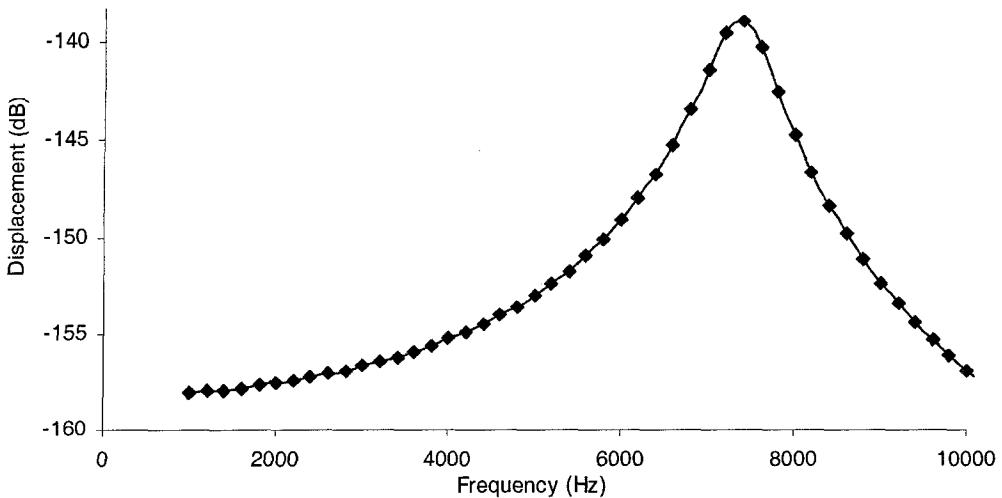
Fig. 4.4: Frequency response of a 7.4 kHz microresonator

As mentioned in chapter 3, a constant edge effect model has been used in which all the dimensions are extended by 4 μm. Fig. 4.4 shows the plot of resonator displacement as a function of frequency. The damping associated with the top surface is not included as the penetration depth at 10 kHz frequency is about 26 μm. This makes the damping associated with the top surface over an order of magnitude smaller than the damping on the bottom surface. This can contribute significantly for frequencies close to 1 MHz. Fig. 4.4 shows the frequency response of a 7.4 kHz microresonator obtained from NODAS simulation. Table 4.1 shows simulated and experimental values of resonant frequency and quality factor for this resonator. Simulation results are in good agreement with the experimental results. The simulated resonant frequency matches to within 1.3% and the simulated Q factor matches to within 8.5% of the experimental values. Table 4.1 also shows the results of microresonators designed for 30 kHz and 100 kHz resonant frequency. It can be seen that the error in the Q value increases with increasing frequency. This can be attributed mainly to two reasons. The constant edge extension model is an approximate model for the edge effects. It's accuracy needs to be verified for frequencies close to 100 kHz. The damping on the top surface (exposed to atmosphere) that is not taken care of in the schematic contributes to the overall damping.

Table 4.1: Resonant frequency (f_r) and quality factor (Q) for different microresonators

design frequency	f_r (experiment	Q (experiment)	f_r (NODAS)	Q (NODAS)
10 kHz	7.4 kHz	8.3	7.31 kHz	9
30 kHz	22.7 kHz	25.6	21.9 khz	31.6
100 kHz	74.1 kHz	80	72.6	130

5. Conclusions and future work

This thesis describes behavioral models for squeeze film and slide film damping in MEMS devices. The models are parameterized and can be used in mixed domain system level simulation of MEMS. It is shown that the edge-effects contribute significantly to the overall damping for plate sizes <50 μm on a side. Extension of the plate edges, as one of the possible ways to model the edge-effects, is discussed. The edge effect model is derived for the case of squeeze film for gaps in the range of 1 μm to 5 μm, plate sizes in the range of 5 μm to 100 μm. For slide films, it is shown that the edge effects are dependent on both the aspect ratio and the orientation of the slide film. Gas rarefaction effects have been modeled using an effective viscosity model.

To show the utility of the models in modeling the damping dynamics, results of system level simulations have been presented and experimentally validated. With these models the designer will be able to model the squeeze film and the lateral (slide film) damping with adequate accuracy.

There are several directions for future work. The presence of holes in the microstructure significantly alters the damping force on the oscillating structure. The effect of the hole size and the hole density on the damping force needs to be studied. A constant edge extension model has been used to model the edge-effects in lateral damping. The gap and plate-size dependent edge effect model derivation can extend the accuracy of the edge-effect model to wider range of input parameters. The effect of the thickness of the oscillating plate on the squeeze film and lateral damping needs to be assessed. The study of the effect of the presence of other static or moving structures near a squeeze film or a slide film can be useful in understanding the damping in case of complex geometries.

References

[1] J. J. Blech, "On Isothermal Squeeze Films", *Journal of Lubrication Technology*, V. 105, 1983, pp. 615-620.

[2] J. B. Starr, "Squeeze Film Damping in solid State Accelerometer", *Tech Digest, IEEE Solid State Sensor and Actuator Workshop*, Hilton Head Island, SC, USA, June 1990, pp.44-47.

[3] T. Veijola, H. Kuisma, J. Lahdenpera, and T. Ryhenen, "Equivalent-Circuit Model of the Squeezed Gas Film in a Silicon Accelerator", *Sensors and Actuators A*, vol. 48, 1995, pp.239-248.

[4] CFD-VIEW, CFD-GEOM, CFD-GUI User Manuals, CFDRC, Huntsville, AL.

[5] M. Torowski, Z. Chen, A. prezekwas, "High Fidelity and Behavioral Simulation of Air Damping in MEMS", *Proc. MSM '99*, pp. 241-244.

[6] E. S. Kim, Y. H. Cho, and M. U. Kim, "Effect of holes and edges on the squeeze film damping of perforated mico-mechancial structures", *IEEE Int. Conf. MEMS*, 1999, pp. 206-301.

[7] S. Vemuri, G. K. Fedder, T. Mukherjee, "Low-Order Squeeze Film Model of Simulation of MEMS Devices", *Proc. MSM*, 2000.

[8] Verilog-A reference Manual.

[9] J. E. Vandemeer, "Nodal Design of Actuators and Sensors (NODAS)", M.S. Thesis, Carnegie Mellon University, 1998.

[10] G. K. Fedder, Q. Jing, "A Hierarchical Circuit-level Design Methodology for Micormechanical Systems", *Trans. Circuits and Systems II*, TCAS 1999.

[11] MAST Reference Manual, Release 4.2, Analogy Inc., Beaverton, OR, 1997.

[12] T. Veijola, T. Ryhänen, H. Kuisma, and J. Lahdenperä, "Circuit Simulation Model of Gas Damping in Microstructures With Non-Trivial Geometries," *Transducers'95 - Eurosensors IX*, Stockholm, June 1995.

[13] Y. H. Cho, B. M. Kwak, A. P. Pisano, and R. T. Howe, "Slide film damping in laterally driven microstructures", *Sensors and Actuators A*, vol. 40, 1994, pp. 31-39.

[14] T. Veijola, "Compact Damping Models for Lateral Strucutres Including Gas Rarefaction Effects", *Proc. MSM*, 2000.

[15] X. Zhang, and W. C. Tang, "Viscous Air Damping in laterally Driven Microstructures", *Sensors and Materials*, vol. 7, No. 6, 1995, pp. 415-430.

[16] Q. Jing, H. Huo, T. Mukherjee, L. R. Carley, and G. K. Fedder, "CMOS Micromechanical Bandpass Filter Design using a hierarchical MEMS Circuit Library", *IEEE Int. Conf. MEMS*, 2000.

[17] T. Mukherjee, S. Iyer, G. K. Fedder, "Optimization-based synthesis of microresonators", *Sensors and Actuators A 70*, 1998, pp. 118-127.

Appendix

The equation for slide film damping coefficient including the gas rarefaction effects is:

$$\bar{\xi} = \frac{\eta_{eff}A}{v}\left.\frac{\partial v(z)}{\partial z}\right|_{z=0} = \eta_{eff}Aq\frac{\cosh(qg) + \hat{q}\lambda\sinh(qg)}{(1+q^2\lambda)\sinh(qg) + 2\hat{q}\lambda\cosh(qg)}$$

The numerator and the denominator are odd functions in the complex frequency variable q and hence have only odd powers in their taylor series expansion in q about $q=0$.

Let the numerator be N(q) and the dominator be D(q). The taylor series expansion of N(q)/ $(\eta_{eff}A)$ is:

$q+q^3(g^2/2+g\lambda)+q^5(g^4/24+g^3\lambda/6)+q^7(g^6/720+g^5\lambda/120)+q^9(g^8/40320+g^7\lambda/5040)+q^{11}(g^{10}/$ $3628800+g^9\lambda/362880)+O[q^{13}]$.

Similarly the denominator D(q) is given by:

$q(g+2\lambda)+q^3(g^3/6+g^2\lambda+g\lambda^2)+q^5(g^5/120+g^4\lambda/12+g^3\lambda^2/6)+q^7(g^7/5040+g^6\lambda/360+g^5\lambda^2/$ $120)+q^9(g^9/362880+g^8\lambda/20160+g^7\lambda^2/5040)+q^{11}(g^{11}/39916800+g^{10}\lambda/1814400+g^9\lambda^2/$ $362880)+O[q^{13}]$.

The ratio of the two series has only even powers of q in the numerator and denominator as in:

$$\bar{\xi} = \frac{\sum\limits_{\substack{i=0 \\ even}}^{\infty} n_i q^i}{\sum\limits_{\substack{i=0 \\ even}}^{\infty} d_i q^i}$$

The Coefficients n_i and d_i are as in the above mentioned series.